Role of gut-liver axis in circadian exercise and dietary interventions to improve metabolic health

Kovynev, A.S.

Chapter 4

Timing matters: Late, but not early, exercise training ameliorates MASLD in part by modulating the gut-liver axis in mice

Timing matters: Late, but not early, exercise training ameliorates MASLD in part by modulating the gut-liver axis in mice

Artemiy Kovynev[1,2], Zhixiong Ying[1,2]*, Sen Zhang[1,2], Emanuele Olgiati[1,2], Joost M. Lambooij[3,4], Clara Visentin[1,2], Bruno Guigas[3], Quinten R. Ducarmon[3], Patrick C.N. Rensen[1,2] and Milena Schönke[1,2$]*

[1]Division of Endocrinology, Department of Medicine, Leiden University Medical Center, Leiden, The Netherlands
[2]Einthoven Laboratory for Experimental Vascular Medicine, Leiden University Medical Center, Leiden, The Netherlands
[3]Leiden University Center for Infectious Diseases (LUCID), Leiden University Medical Center, Leiden, The Netherlands
[4]Department of Cell and Chemical Biology, Leiden University Medical Center, Leiden, The Netherlands

**Contributed equally*
$ Dr. Milena Schönke is the corresponding author. Email: m.schoenke@lumc.nl

Data availability

16S and metagenomics data are available from the ENA database (ascension number PRJEB78442).

Funding declaration of interests

This work was supported by the Novo Nordisk Foundation (grant NNF18OC0032394 to M.S.), The Netherlands Cardiovascular Research Initiative CVON-GENIUS-2 (grant to P.C.N.R.), the Chinese Scholarship Council (grants to Z.Y. and S.Z.). A.K. is supported by a PhD grant from Leiden University Medical Center (to M.S.).

Declaration of interests

The authors declare that the research was conducted in the absence of any commercial or financial relationships that could be construed as a potential conflict of interest.

Abstract

Background: Metabolic dysfunction-associated steatotic liver disease (MASLD) affects two billion people worldwide and is currently mostly treatable via lifestyle interventions, such as exercise training. However, it is unclear whether the positive effects of exercise are restricted to unique circadian windows. We therefore aimed to study whether the timing of exercise training differentially modulates MASLD development.

Methods: Twenty weeks old male APOE*3-Leiden.CETP mice were fed a high fat-high cholesterol diet to induce MASLD and treadmill-trained for one hour five times per week for twelve weeks either early (ZT13; E-RUN) or late (ZT22; L-RUN) in the dark phase, while corresponding sedentary groups (E-SED and L-SED) did not. To assess the role of the gut microbiota in training-induced effects, the study was repeated and trained (ZT22 only, RUN) or sedentary mice (SED) served as fecal donors for sedentary recipient mice (RUN FMT and SED FMT).

Results: Late, but not early exercise training decreased the MASLD score, body weight, fat mass, and liver triglycerides, accompanied by an altered composition of the gut microbiota. Specifically, only late exercise training increased the abundance of short-chain fatty acid-producing bacterial families and genera, such as *Akkermansia, Lachnospiraceae* and *Rikenella*. Fecal microbiota transplantation reduced liver weight and plasma triglycerides in RUN FMT compared to SED FMT, and tended to lower the MASLD score and liver triglycerides.

Conclusion: Timing of exercise training is a critical factor for the positive effect on MASLD in this pre-clinical model, and the effect of late exercise is partially mediated via the gut-liver axis.

Keywords: MASLD, circadian rhythms, exercise, gut microbiota, mouse model

Introduction

Metabolic dysfunction-associated steatotic liver disease (MASLD, formerly known as NAFLD) is a major public health burden that affects more than 30% of the global population, and its prevalence is predicted to increase further in the future[1,2]. MASLD is characterized by a prolonged accumulation of lipid droplets in the liver, which is generally a result of excessive caloric intake[3]. This accumulation induces the release of pro-inflammatory signals, promoting an influx of immune cells into the liver and an advancement of the disease to metabolic dysfunction-associated steatohepatitis (MASH), which may lead to liver fibrosis. Gut-liver axis dysfunction has recently emerged as an additional MASLD contributor, with changes in the composition and function of the gut microbiota leading to higher energy harvesting and lipid absorption and an increased influx of pro-inflammatory molecules into the liver[4]. Liver steatosis and MASH are reversible, but pharmaceutical treatment options are currently limited, with the first anti-MASLD treatment having been conditionally approved by the USA Food and Drug Administration only this year[5]. As a result, the most common viable treatment strategies are lifestyle interventions, such as dietary changes and increasing physical activity. It is crucial to optimize such interventions to maximize their effectivity[6].

One potential way of maximizing intervention effectivity is the choice of an appropriate circadian window for exercise. Nearly all processes in the body are controlled by circadian rhythms[7]. In addition to the central clock in the hypothalamus, organs have their own peripheral circadian clocks in order to optimize their function[8]. MASLD dampens the circadian rhythmicity of cellular processes in the gut and the liver, leading to increased metabolic disturbances, while exercise training can contribute to “fine-tuning” of the clock, at least in skeletal muscle[8,9] and liver[10,11]. However, it remains unclear what the optimal training time is for the treatment and prevention of MASLD. In patients with obesity and type 2 diabetes, late exercise training improves glycemic control, whereas early exercise training causes unfavorable spikes in glycemia[12]. Epidemiological studies show that increased afternoon physical activity decreases the risk of cardiometabolic diseases compared to morning physical activity in the Netherlands Epidemiology of Obesity cohort[13], even though the contrary was observed in a comparable sedentary and overweight population from the UK Biobank[14]. In mice, we have previously shown that only late, but not early exercise training reduces the development of atherosclerosis[15], a disease closely related to MASLD in

pathogenesis. Surprisingly, in mild MASLD, early exercise training promotes the influx of pro-inflammatory cells into the liver, which is normally observed with disease progression, while late exercise training does not[16]. Additionally, we identified an enrichment of potentially health-promoting gut bacteria uniquely with late exercise training in mice[15].

Disturbances in the gut-liver axis have been implicated in multiple cardiometabolic diseases[17]. In humans, Western diet decreases the microbial diversity in the gut and reduces the abundance of *Ruminococcaceae* and *Bifidobacterium*, two bacterial taxa associated with decreased liver fibrosis[17]. Western diet also increases bacterial ethanol production, leading to higher energy harvesting and, as a result, increases calorie absorption from the consumed food[17,18]. Furthermore, these changes lead to a leakier gut barrier due to impaired tight junctions between enterocytes[19]. As a result, more microbial molecules such as lipopolysaccharide (LPS) can reach the bloodstream and increase hepatic and systemic inflammation[17,19]. Finally, high-fat diet decreases the amount of short-chain fatty acid (SCFA)-producing bacteria and specifically butyrate producers, which is generally associated with an unfavorable disease outcome[17]. Consequently, addressing gut dysbiosis in MASLD via lifestyle interventions may be a step forward to ameliorating disease progression.

In the current study, we investigated the influence of early and late active period exercise training on the amelioration of MASLD in high fat-high cholesterol (HFHC) diet-fed male APOE*3-Leiden.CETP mice, a model mimicking human MASLD development[20].

Materials and methods

Animal experiments

Male APOE*3-Leiden.CETP mice were bred as previously described[21]. In experiment 1, mice at the age of 20 to 26 weeks were group housed (two to four mice per cage) under standard conditions (22°C, 12/12 hours light/dark cycle; the light phase started at *Zeitgeber* time/ZT 0) with *ad libitum* access to water and a high-fat high-cholesterol (HFHC) diet (60 kJ% fat + 1% w/w cholesterol; D12492, ssniff Spezialdiäten GmbH, Soest, Germany). Cages were enriched with cardboard rolls, nesting material and a wooden stick for chewing. After three weeks of dietary acclimatization, based on body weight, body composition and 4-hour fasted plasma triglyceride (TG) and total cholesterol (TC) levels, mice were randomized into four

treatment groups (n=18 per group, in total 72 animals) using RandoMice version 1.0.9[22]. Two groups exercised on a treadmill at the same running speed five consecutive days per week (Monday to Friday) for twelve weeks either at ZT13 ("early runners", E-RUN) or at ZT22 ("late runners", L-RUN) for one hour, while early and late sedentary mice (E-SED and L-SED, respectively) were picked up, put on the researcher's hand and returned to their home cages at the beginning of the running bout of their exercising counterparts to account for handling stress (Figure 1A). At the end of the experiment, all mice were fasted for four hours and sacrificed at ZT18; therefore, E-RUN and L-RUN mice were killed 28 and 19 hours after their last exercise training, respectively. The same ZT time of sacrifice for all groups was chosen to eliminate the circadian oscillations bias, with ZT18 being between the two training timepoints. Five mice per group received an oral gavage of FITC-Dextran three hours into the fasting period (see section "Intestinal permeability measurement", Supplementary information), and another five mice per group received an intravenous injection of glycerol tri[^{3}H]oleate ([^{3}H]triolein; [^{3}H]TO)-labeled TG-rich lipoprotein (TRL)-like particles) together with [^{14}C]deoxyglucose after the fast (see section "*In vivo* organ uptake of TRL-mimicking particles and glucose", Supplementary document 2). The remaining eight mice per group did not receive any treatment, and their immune cells were isolated from liver and used for flow cytometry analysis (see section "Liver immune cell isolation and flow cytometry", Supplementary document 2). The mice used for each treatment were matched by body mass, fat mass and plasma TG levels. All mice were sacrificed by CO_2 asphyxiation before portal vein blood (only in mice used for immune cell isolation) and heart puncture blood was collected, and the animals were perfused with PBS (ice-cold for all mice except the ones used for flow cytometry analysis) and multiple organs (liver, gonadal white adipose tissue (gWAT), subcutaneous white adipose tissue (sWAT), interscapular brown adipose tissue (iBAT), quadriceps, tibialis anterior (TA) muscle, gastrocnemius muscle, as well as caecum and caecum content) were collected. Four mice were excluded due to tumors/cysts in different parts of the body.

In experiment 2 (timeline overview in Suppl. Figure 6A), male APOE*3-Leiden.CETP mice at the age of 10 to 14 weeks were housed under the same conditions and fed with the same HFHC diet as in experiment 1. After three weeks of dietary acclimatization, mice were divided into fecal microbiota donors and fecal microbiota recipients. Donors either exercised on the treadmill five times per week

for twelve weeks (RUN group) or were handled (SED group) at ZT22 (n=20 per group, in total 80 animals) as described. From four weeks of training onwards, fresh feces were collected from the donors and pooled per group for fecal microbiota transplantation (FMT) three times per week for eight weeks, leading to the recipients being divided into a RUN FMT group and a SED FMT group (n=20 per group) (Figure 5A). Two weeks prior to the FMT, recipients were subjected to antibiotics treatment for two weeks to diminish the endogenous gut microbiota and improve FMT engraftment (see sections "Antibiotic treatment" and "Fecal microbiota transplantation", Supplementary document 2). All mice were sacrificed at ZT18 by CO_2 asphyxiation before portal vein blood and heart puncture blood was collected, the animals were perfused with ice-cold PBS, and multiple organs were collected as described above.

All procedures are described in detail in the Supplementary document 2. We used the ARRIVE[23] checklist when writing our report.

Ethics statement

All animal experiments were carried out according to the Institute for Laboratory Animal Research Guide for the Care and Use of Laboratory Animals, and were approved by the National Committee for Animal Experiments (Protocol No. AVD 11600202010187) and by the Ethics Committee on Animal Care and Experimentation of the Leiden University Medical Center (Protocols No. PE.21.002.029 and PE.21.002.057 for the first and second animal experiment, respectively).

Statistical analysis

All individual data points are shown and data are expressed as mean ± SEM. Statistical analyses were performed using GraphPad Prism 9.01 (GraphPad, La Jolla, California) and one-way ANOVAs followed by Tukey's multiple comparisons test where appropriate. The data were tested for normality and all data sets were normally distributed. Statistical outliers were removed after identification by Grubb's test (α=5%). Differences between groups were considered statistically significant if $p < 0.05$ (*), $p < 0.01$ (**), $p < 0.001$ (***) or $p < 0.0001$ (****).

Results

Only late, but not early exercise training reduces body weight gain

To investigate the impact of timed exercise training on the development of MASLD, male APOE*3-Leiden.CETP mice were fed a HFHC diet and exercise trained five times per week for twelve weeks either at ZT13 (E-RUN) or ZT22 (L-RUN), equivalent to the human morning and evening (Figure 1A). Exercise training at either ZT13 or ZT22 did not affect food intake (Figure 1B, Suppl. Figure 1A, B). E-RUN gained less body weight from week 5 to 10, but caught up by week 12 as compared to E-SED (Figure 1C). On the other hand, late exercise training attenuated body weight gain throughout the study (Figure 1C). By week 12, E-RUN had a higher lean mass than E-SED, while there was no difference between L-RUN and L-SED (Figure 1D, Suppl. figure 1C). Both early and late exercise training led to a smaller fat mass by week 12 as compared to their sedentary counterparts. However, the difference reached statistical significance only with late exercise training (Figure 1E, Suppl. figure 1D). In line, the weight of sWAT was lower in both exercise training groups (Figure 1F). Both early and late exercise training decreased levels of plasma TG and TC as compared to their respective sedentary controls (Figure 1G, H). Taken together, both early and late exercise training showed positive effects on overall health, but late exercise training more effectively attenuated body weight gain.

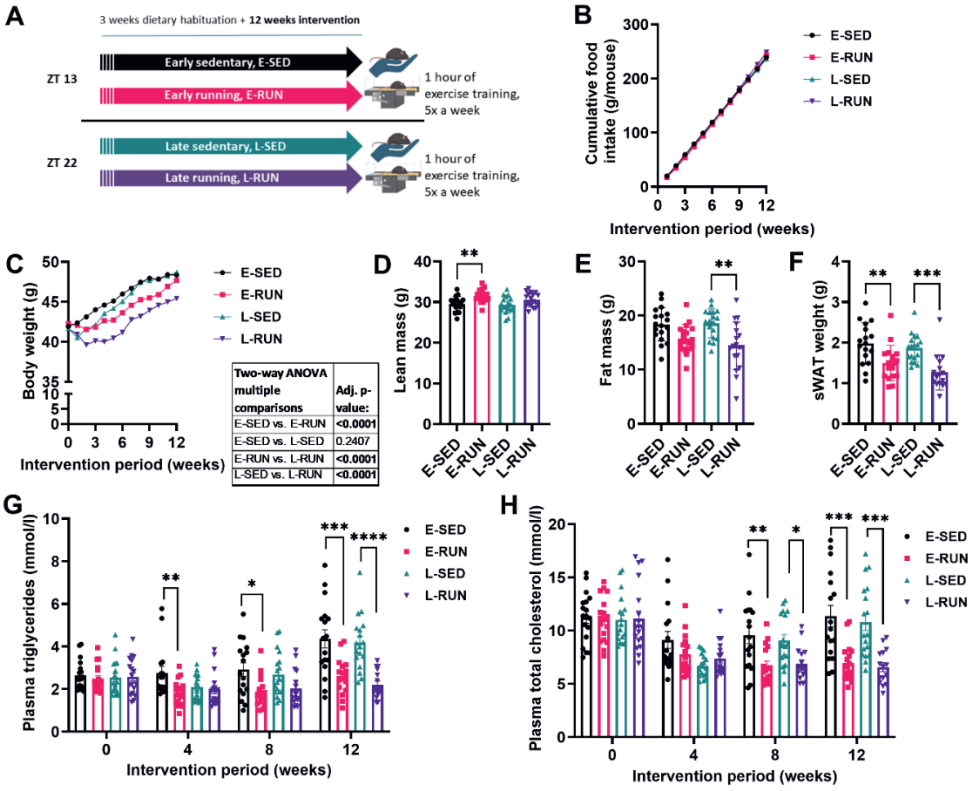

Figure 1. Effect of early and late exercise training on body composition and plasma lipids. (**A**) MASLD-prone male APOE*3-Leiden.CETP mice on a HFHC diet were treadmill-trained five times per week either in the early (Zeitgeber time/ZT 13) or late (ZT 22) dark phase for 12 weeks. (**B**) Cumulative food intake and (**C**) body weight gain were assessed throughout the study, and (**D**) lean mass, (**E**) fat mass and (**F**) subcutaneous white adipose tissue (sWAT) mass were measured at endpoint. (**G**) Plasma triglycerides and (**H**) total cholesterol levels were assessed throughout the study. Data are presented as mean ± SEM (n = 16–18), *p < 0.05, **p < 0.01, ***p < 0.001 according to one-way ANOVA (D-F) or two-way ANOVA (B, C, G, H) followed by Tukey multiple comparison test.

Only late, but not early exercise training alleviates liver steatosis

In order to evaluate the effects of early and late exercise training on the amelioration of MASLD, we next assessed liver health and lipid accumulation. L-RUN but not E-RUN showed smaller liver sizes as compared to their corresponding sedentary counterparts (Figure 2A). Strikingly, this late exercise-specific benefit was also observed when assessing the MASLD score, where L-RUN showed a lower score than L-SED while the scores of E-RUN did not differ from E-SED (Figure 2B, C). This was mainly explained by less macrosteatosis and hepatocyte hypertrophy in L-RUN (Suppl. figure 2A-C). These results were further supported by biochemical measurements showing that hepatic TG content was only lowered by late, but not early exercise training (Figure 2D). Hepatic cholesterol content, on the other hand, was decreased in both E-RUN and L-RUN compared to the corresponding SED groups (Figure 2E). To investigate the underlying cause for the improved hepatic steatosis with late exercise training, we quantified the organ uptake of lipids and glucose using [^{3}H]TO-labeled TRL-like particles and [^{14}C]deoxyglucose. Here, only late exercise training tended to decrease the uptake of [^{3}H]TO and [^{14}C]deoxyglucose by the liver (Suppl. figure 2E, F). We did not observe differences in the uptake of these tracers by adipose tissue or skeletal muscle (Suppl. figure 3A-H). We next measured the expression of hepatic genes related to fatty acid and bile acid metabolism. No changes between groups were observed in the expression of genes associated with *de novo* lipogenesis (*Srebp1c* and *Fasn*), fatty acid uptake (*Cd36*) and oxidation (*Cpt1a*) (Figure 2F). The expression of *Cyp7a1* and *Cyp7b1*, encoding key enzymes in the primary bile acid synthesis pathways, was upregulated by only late training and by both late and early training, respectively (Suppl. figure 2G-L). Despite the unchanged lipid and glucose uptake by adipose tissue and unchanged adipocyte sizes (Suppl. figure 3I), both exercise groups showed fewer crown-like structures in sWAT, a marker of tissue inflammation (Suppl. figure 3J). Finally, because of the absence of changes in tracer uptake by muscle, we measured the abundance of mitochondrial respiratory complexes in the skeletal muscles to quantify muscle oxidative capacity in the mice subjected to the differently timed exercise regimens. There was no change in the protein abundance between the groups (Suppl. Figure 3K-Q). Taken together, only late exercise training ameliorated liver steatosis in conjunction with changes in hepatic energy uptake.

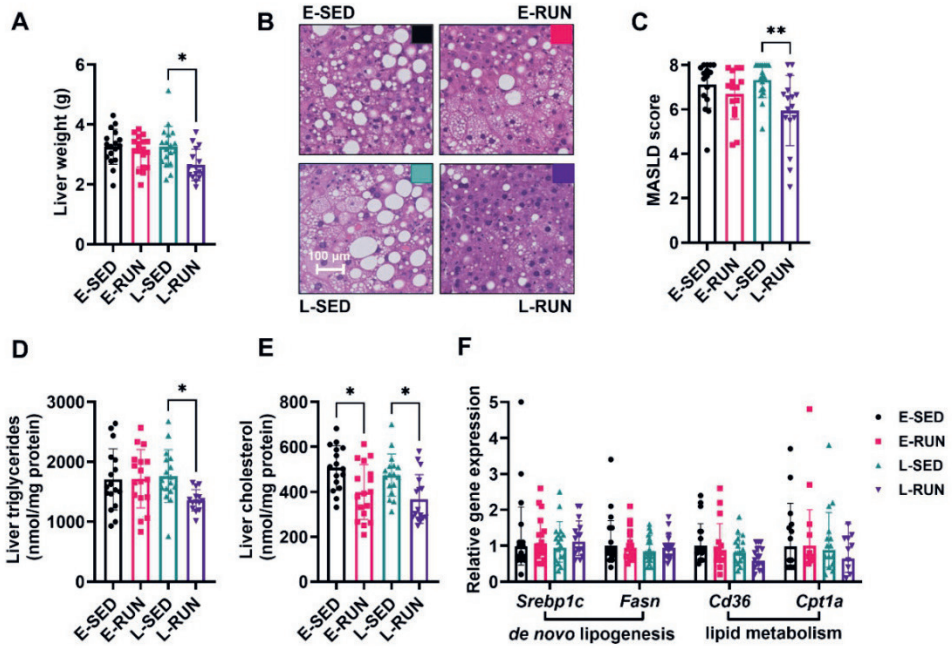

Figure 2. Effect of early and late exercise training on liver steatosis. At the end of the 12-week experiment, (**A**) liver weight was measured and (**B-C**) MASLD score was determined on H&E stained liver sections. The liver content of (**D**) triglycerides and (**E**) total cholesterol was assessed, and (**F**) the expression of genes related to lipid metabolism were measured in the liver. *Srebp1c*, sterol regulatory element-binding protein 1 c; *Fasn,* fatty acid synthase; *Cd36*, cluster of differentiation 36; *Cpt1a*, carnitine palmitoyltransferase 1α. Data are presented as mean ± SEM in **A-B** and **D-E** or as geometric mean ± geometric SD in **F** (n = 16–18). *p < 0.05, ****p < 0.0001 according to one-way ANOVA followed by Tukey's multiple comparison test.

Exercise training regardless of timing attenuates inflammation and fibrosis in the liver

Next, we investigated the inflammatory and fibrogenic processes that drive MASLD progression. As determined in H&E-stained liver sections and similarly to attenuated inflammation in white adipose tissue, the inflammation score was similarly lowered in E-RUN and L-RUN compared to their sedentary counterparts (Suppl. Figure 2D). In line, the hepatic abundance of F4/80 protein, a marker of

murine macrophages, was lowered in both exercise training groups (Figure 3A, B). The expression of *Adgre1*, which encodes F4/80, only tended to decrease upon late exercise training, while in line with the previous observations, the mRNA expression level of *Tnfa*, encoding a main inflammatory cytokine secreted by macrophages, was decreased in both exercise training groups (Figure 3C). The expression of *Il1b,* another pro-inflammatory cytokine, was not affected (Figure 3C). This anti-inflammatory effect of exercise was further supported by flow cytometry data (Suppl. figure 4A-X) showing that both early and late exercise decreased the number of $CD11C^+$ cells, a marker of MASLD progression, in a subset of macrophages (Suppl. figure 4T, V, X). To assess the impact of the exercise training on fibrosis development, the hepatic collagen content was determined via histological staining and found to be decreased in both E-RUN and L-RUN compared to their corresponding sedentary controls (Figure 3D, E). In line, the gene expression of *Col1a1*, which encodes the major component of type I collagen, was found to be downregulated in both exercise training groups (Figure 3C). Together, these results demonstrate that exercise training independently of timing attenuates inflammation and fibrogenesis in the liver.

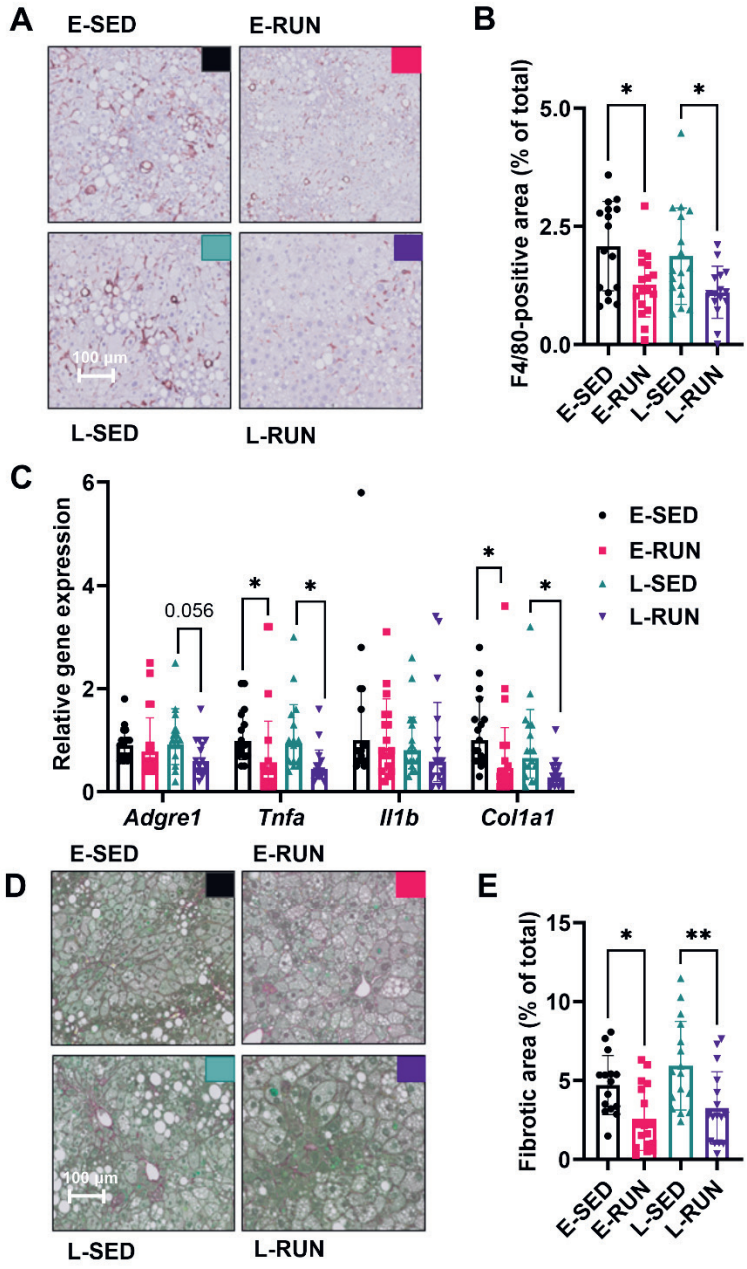

Figure 3. Effect of early and late exercise training on liver inflammation and fibrogenesis. After 12 weeks of exercise training, (**A-B**) hepatic macrophages were visualized with an F4/80 staining. (**C**) The gene expression of pro-inflammatory and pro-fibrotic markers was measured and (**D-E**) liver fibrosis was quantified with a

Sirius red/Fast green staining. Data are presented as geometric mean ± geometric SD in **C**, and as mean ± SEM (n = 16–18) in **B** and **E**, *p < 0.05, ***p < 0.01 according to one-way ANOVA followed by Tukey's multiple comparisons test.

Only late, but not early exercise training reshapes gut microbiota composition

Since MASLD is modulated by gut dysbiosis, we next investigated whether the underlying mechanisms of the effect of late exercise training on MASLD are associated with microbiota changes. For this, we performed 16S sequencing of mouse caecum content. Neither early nor late exercise training changed the α-diversity, a measure of bacterial community richness (Suppl. figure 5A). Late exercise training, however, led to a shift in microbial composition as reflected by a different β-diversity of L-RUN compared to L-SED, while this was not seen for E-SED and E-RUN (Suppl. figure 5B). To further investigate what constitutes this microbial shift, we investigated the changes in the relative abundance of bacteria on phylum, family and genus levels. On the phylum level, *Firmicutes* increased significantly in L-RUN compared to L-SED, with no other significant changes (Figure 4A). On the family level, *Clostridia_vadinBB60_group* increased 4-fold in L-RUN compared to both L-SED and E-RUN (Suppl. figure 5C). On the genus level, both exercise training groups increased the relative abundance of *Lactobacillus* (Figure 4B). Compared to both L-SED and E-RUN, L-RUN decreased the abundance of *Alistipes* (Suppl. figure 5D), while increasing the abundance of *Rikenella* and *Lachnospiraceae UCG-006* (Figure 4B). L-RUN also had an increased abundance of *Acetatifactor* and *Akkermansia* compared to L-SED (Figure 4B). These enriched species are known SCFA producers.

Since 16S sequencing only determines the relative abundance of bacteria with few functional insights and the current murine gut databases leave a large number of unassigned taxa, we conducted shotgun metagenomics sequencing on the combined group of E-SED and L-SED (further referred to as SED) and E-RUN and L-RUN. In agreement with the 16S sequencing data, shotgun metagenomics sequencing revealed a strong shift in β-diversity in only L-RUN compared to both E-RUN and SED (Figure 4C, D), confirming that overall only late exercise training led to changes in the gut microbiota composition. On the genus level, similarly to the 16S sequencing results, exercise training increased the abundance of *Lactobacillus*

which only reached significance for L-RUN (Figure 4E). In line with the 16S sequencing, the abundance of *Alistipes* was dramatically suppressed in L-RUN, with E-RUN following a similar trend, while *Blautia* was only reduced by late exercise training (Figure 4F). Curiously, we found two species, *Lachnospiraceae species i.s.* and *Ruminococcaceae species i.s.* (Figure 4G), constituting 1% of the overall relative abundance, that were only increased in L-RUN. Despite reshaping the gut microbiota, late exercise training did not change the caloric output in the feces or intestinal permeability (Suppl. figure 5E, F).

As we saw an increase in SCFA producers in the gut, we quantified SCFA levels in the plasma of portal vein blood, which transports intestine-derived SCFAs to the liver, collected 19-28 hours after the last training bout following four hours fasting. While total SCFA levels (Figure 4H) that primarily reflected the abundance of acetate (Suppl. figure 5H), tended to be mildly increased in both exercising groups, there was no significant difference between the groups (Suppl. Figure 5G, I-M). Curiously, despite a lack of significant difference in concentration between the exercise training groups, the total concentration of SCFAs in portal vein blood plasma negatively correlated with the steatosis MASLD score (Figure 4I). Additionally, the abundance of the *Lachnospiraceae* family, of which several members were increased only in the L-RUN, correlated positively with the total SCFAs concentration in the portal vein plasma (Figure 4J). Taken together, these findings indicate that the reshaping of the gut microbiota with late exercise training may play a role in attenuating MASLD development.

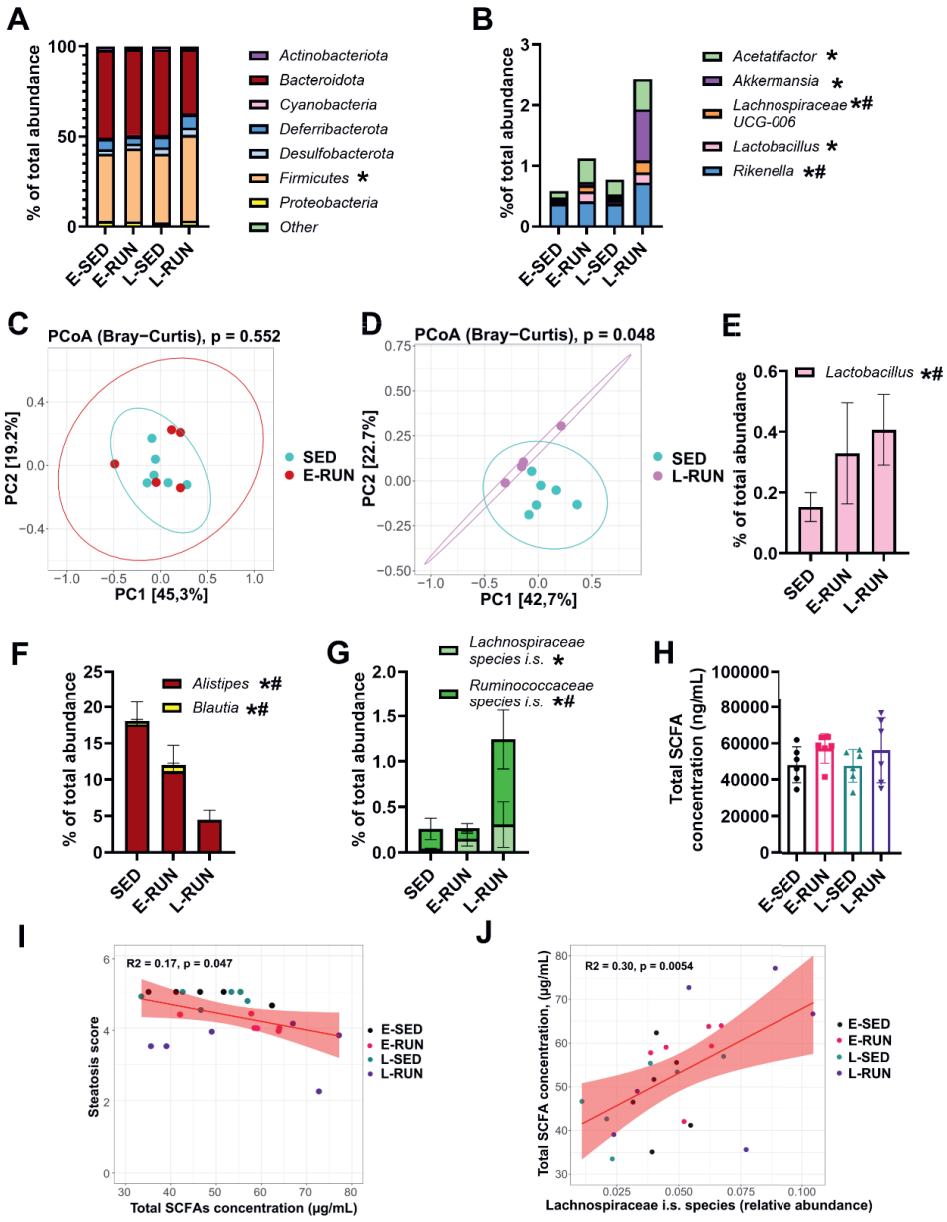

Figure 4. Effect of early and late exercise training on gut microbiota composition. 16S sequencing of the cecum content was conducted after 12 weeks of training and the abundance of (**A**) bacterial phyla and (**B**) genera was quantified. Data are presented as mean (n = 16–18), *L-RUN vs L-SED, #L-RUN vs E-RUN, according to Wald test with FDR set to 0.05. In depth metagenomics sequencing of a subset of

samples was conducted and (**C-D**) the β-diversity Bray-Curtis dissimilarity index calculated and groups compared with PERMANOVA. The abundance of genera (**E**) increased and (**F**) decreased in the L-RUN group was quantified, as well as (**G**) species increased in the L-RUN group. Data are presented as mean ± SEM (n = 4-6), *L-RUN vs L-SED, #L-RUN vs E-RUN, according to Wald test with FDR set to 0.05. Total SCFA concentration was measured in the portal vein blood plasma (**H**) and correlated to steatosis score (**I**) and the relative abundance of the identified increased bacterial species (**J**). Data are presented as mean ± SEM (n = 5-6) in (**H**) according to one-way ANOVA, and as a correlation plot according to Pearson correlation test (**I-J**).

Fecal microbiota transplantation from late-trained mice tends to decrease liver lipid accumulation

To investigate if the gut microbiota changes observed with late exercise training are causal for the MASLD amelioration, we conducted an FMT experiment. Antibiotic-treated male APOE*3-Leiden.CETP mice received FMT from either sedentary (SED) mice or mice trained at ZT22 (RUN) for eight weeks (Figure 5A). This experiment confirmed the beneficial effects of late exercise training on body weight and fat mass gain, plasma TG and TC levels and liver size in RUN mice (Figure 5B-G), as observed in experiment 1. Although not statistically significant, there was a clear trend for RUN FMT attenuating weight gain and plasma TG levels when compared with SED FMT (Figure 5D), while only exercise training itself decreased plasma TC in RUN (Figure 5E). Importantly, RUN FMT mice tended to have a lower liver weight (Figure 5F) and had a significantly lower liver/BW ratio similarly to RUN (Figure 5G). In line, both RUN and RUN FMT showed a reduced liver TG content compared to SED (Figure 5H). However, despite an approximate 15% decrease, there was no significant difference between RUN FMT and SED FMT, due to a large intra-group variability (Figure 5H). Histological analysis of the livers showed similar results, with a decreased MASLD score in RUN and a trend towards a reduced score in RUN FMT compared to the corresponding SED and SED-FMT groups (Figure 5I, J, Suppl. figure 6B). Similarly, a lipid staining of the liver showed a decrease in lipid accumulation in both RUN and RUN FMT compared to SED, but no significant difference compared to SED FMT (Figure 5K-L). Curiously, only RUN decreased inflammation in the liver based on the histological inflammation score and the gene expression levels of pro-

inflammatory cytokines, with no inflammatory changes in RUN FMT (Suppl. figure 6C, D). These findings suggest that microbiota transplantation from trained into untrained mice confers some of the beneficial effects of late exercise training on the liver and whole body, but with greater intra-group variability.

FMT leads to an intestinal passage effect rather than stable engraftment of transplanted bacteria

While RUN FMT tended to improve overall metabolic and liver health, it is still unclear which bacteria or metabolites contributed to these changes. To investigate this further, we conducted 16S sequencing on representative cecum content samples of the donor and recipient mice. The antibiotics treatment prior to the FMT successfully depleted the gut microbiota of the recipient mice, clearly decreasing the Shannon diversity index from 3.2±0.1 before the antibiotics treatment to 1.4±0.3 after antibiotics (Figure 5M). The analysis of the β-diversity also showed a change after the antibiotics treatment (Suppl. figure 6E). However, at the end of the study, only RUN showed a significantly different gut microbiota composition from both SED and RUN FMT, while there was no difference in β-diversity between SED FMT and RUN FMT (Figure 5 N-Q). When dividing the RUN FMT mice into mice with high and low liver TG and MASLD score, mice with low TG and MASLD score (responders) had a similar microbiota composition to RUN mice, while mice with high liver TG and MASLD score had a composition more similar to SED (Figure 5R). This indicates that the success of the FMT engraftment varied and only a successful engraftment replicated the observed MASLD amelioration achieved by exercise training.

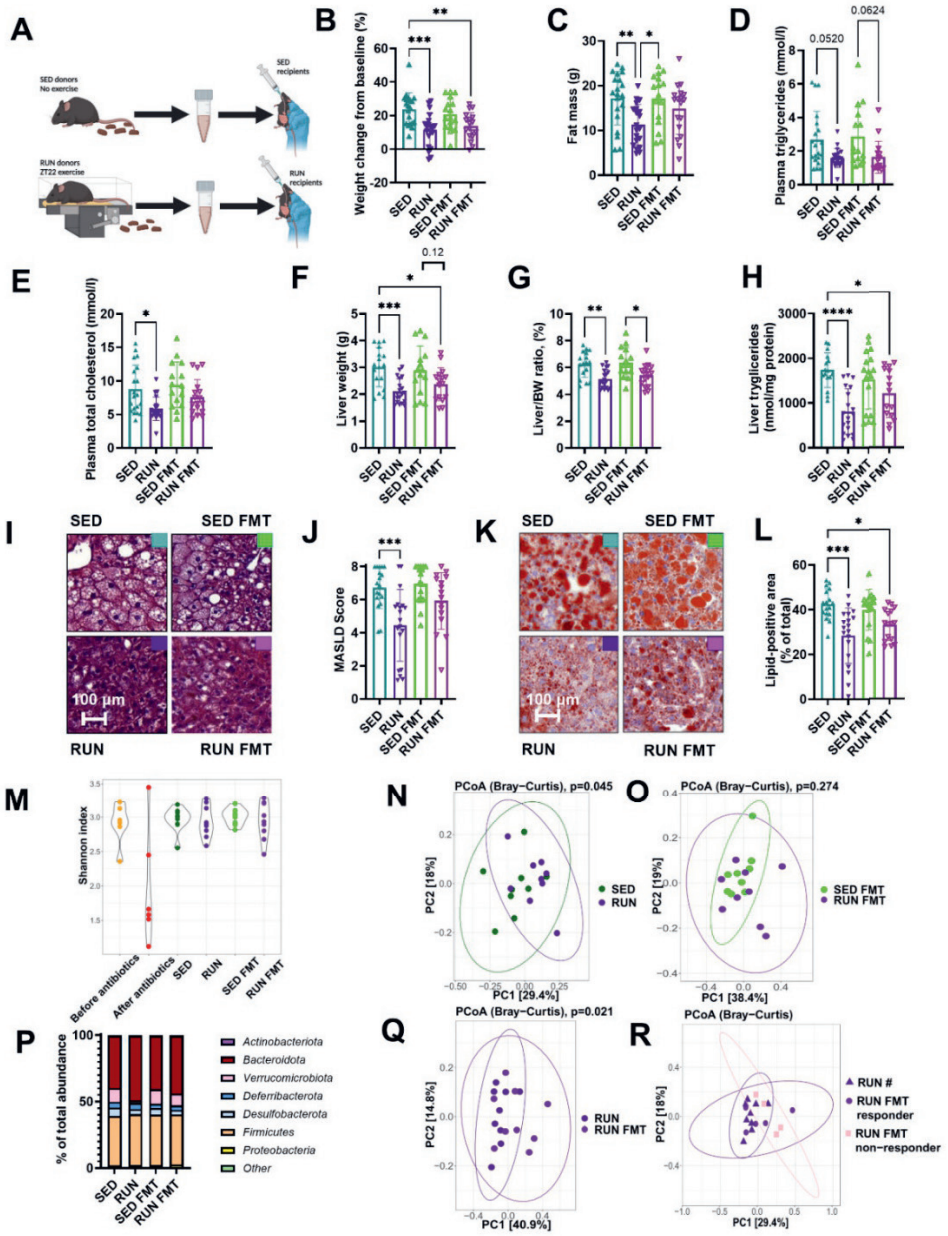

Figure 5. The effect of fecal microbiota transplantation from late-trained into untrained mice on MASLD amelioration. (**A**) Feces from sedentary (SED) and late - trained (RUN) mice were transplanted to corresponding sedentary groups (SED FMT and RUN FMT) for eight weeks. At the end of the experiment, (**B**) weight

change, (**C**) fat mass, (**D**) plasma triglycerides and (**E**) total cholesterol were quantified. To investigate liver changes, (**F**) liver weight, (**G**) liver to body weight ratio and (**H**) liver triglycerides were measured, (**I**) H&E staining was performed to calculate (**J**) the MASLD score and (**K**) ORO staining was performed to measure (**L**) the amount of lipids in the liver sections. To investigate microbiota composition changes, 16S sequencing was performed, and (**M**) α-diversity, (**N, O, Q**) β-diversity between groups and (**R**) β-diversity difference between RUN, RUN FMT responders and RUN FMT non-responders was quantified. The phylum abundance (**P**) in the groups was measured. (**B-L**) are presented as mean ± SEM (n = 17–20), *p < 0.05, **p<0.01 ***p < 0.001, ****p<0.0001 according to one-way ANOVA followed by Tukey's multiple comparisons test. Differences between the groups in (**N-O, Q-R**) were calculated with PERMANOVA with Bonferroni correction, with test results shown on top of the panel for **N**, **O** and **Q**, and # showing comparison between RUN and RUN FMT non-responders, where # stands for p<0.05, while differences in (**P**) were calculated according to Wald test with FDR set to 0.05. Unless specified otherwise, only significant comparisons are shown.

Discussion

Exercise interventions are among the few available MASLD treatments, but little is known about optimizing these interventions in conjunction with our circadian rhythm[1,9,24,25]. Here, we demonstrate for the first time in a MASLD mouse model that only late, but not early active phase exercise training effectively ameliorates MASLD development and that this effect is partially mediated via the gut-liver axis.

Clinically, weight loss is instrumental in the MASLD resolution, with already 5% weight loss leading to a significant improvement in steatosis[26]. While we observed a significant weight and fat mass loss with late exercise training that coincided with reduced steatosis, we curiously did not observe any differences in food intake or energy excretion between the groups, suggesting that altered energy utilization is the main mechanism underlying these positive effects of late training. This may be associated with the timing of food intake as the early-trained mice presumably ate the majority of calories after the training, while the late-trained animals ate the bulk before the training. However, as high-fat diet-fed mice have a disrupted circadian feeding rhythm with up to 30% of the food intake taking place during the light phase[27], it is unclear how much feeding timing contributed to the observed effects in this study. Nevertheless, we observed no differences between the groups in

hepatic fatty acid metabolism-related gene expression or liver uptake of lipids or glucose. Since all these measurements were performed at rest 19 to 28 hours after the last training bout, however, it is conceivable that late-trained mice achieved a greater use of energy during exercise but not at rest. While we did not see an increase in the protein abundance of the individual oxidative mitochondrial complexes or an increased uptake of the lipids or glucose by skeletal muscle at rest either, possibly due to samples being collected at ZT18, when muscle oxidative capacity is not at its peak, muscle oxidative capacity has been shown to be increased during training later in the day[28,29]. This suggests greater energy utilization by muscle later in the active phase, especially paired with a possibly increased SCFA influx from the gut[30] which is known to increase muscle oxidative capacity further[31,32]. Hence, we hypothesize that small acute effects during the daily exercise bouts accumulate into major effects after twelve weeks of training that lead to MASLD amelioration with late exercise training.

While only late exercise training reduced liver lipid accumulation, both early and late exercise training decreased markers of hepatic inflammation and fibrogenesis. This suggests that at a MASLD stage with pronounced steatosis and beginning fibrosis, inflammation and fibrogenesis are not regulated by the circadian aspect of exercise, possibly due to strong intra-hepatic disease drivers being not any longer under circadian control. Additionally, while exercise-to-sedentary FMT tended to decrease liver lipid accumulation, it had no effect on liver inflammation, suggesting that the anti-inflammatory effect of exercise training is likely not directly mediated via the gut microbiota. This is in line with our observation that the gut microbiome was only changed in late-trained mice while early-trained mice also showed an amelioration of liver inflammation. Alternatively, this time-independent beneficial effect of exercise on liver inflammation may be explained by a modulation of hepatic cholesterol metabolism, as livers of both early and late exercise-trained mice demonstrated decreased total cholesterol levels. This matches previous studies demonstrating that liver cholesterol is a determinant of liver inflammation[24,33]. In line, the expression of the *Cyp7b1* gene of the alternative bile acid synthesis pathway was elevated in both exercise groups, potentially indicating increased cholesterol excretion in trained animals which in turn alleviates hepatic inflammation and pro-fibrotic processes.

An improved MASLD outcome is usually associated with beneficial changes in the gut microbiota composition in patients with MASLD[34] and establishing a healthy gut microbiota can even counteract weight re-grain in individuals following a lifestyle intervention[35]. In line, we here observe that only late, but not early exercise training modified the gut microbiota composition. A higher abundance of *Firmicutes* as seen in the late-trained animals has been correlated with higher VO_2 max, a marker of oxidative fitness[36-38]. Accordingly, this increase in *Firmicutes* seen with late training may also contribute to the higher exercise capacity humans exhibit later in the day compared to the morning[29]. *Akkermansia*, another genus enriched with late training here, has been linked to the amelioration of atherosclerosis, MASLD and type 2 diabetes, possibly via improved intestinal glucose control[39-42]. Also, *Lactobacillus* has been associated with decreased liver fat, liver cholesterol and overall body fat loss[43-45], possibly via the competition for the available dietary fatty acids in the intestine. *Lachnospiraceae_UCG-006*, here enriched on genus level, has been associated with improved liver health as evident from decreased liver enzyme (ALT and AST) plasma levels in mice[46]. The observed late exercise-induced increase in unidentified members of the *Lachnospiraceae* and *Ruminococcaceae* families is especially interesting, as we have also observed their increase with late exercise training in a hyperlipidemic atherosclerosis-prone mouse model on a Western-type diet[15]. This indicates a robust effect of exercise training on these bacterial species in different mouse models on different diets. These broad families are known to ferment fiber into SCFAs, and SCFAs, especially butyrate, have health benefits, such as improved intestinal epithelial lining integrity, decreased inflammation in the gut and the liver, and increased muscle oxidative capacity[47-50]. In this study, possibly because portal vein blood was collected after 4 hours of fasting one day after the last training bout, we did not see a clear difference in SCFAs levels between groups as they are quickly absorbed. On the other hand, the SCFA levels positively correlated with the abundance of SCFA-producing bacterial species and negatively correlated with MASLD scores. This may hint towards the involvement of SCFAs in MASLD amelioration in the current study and towards an effect that carries over into periods of rest from acute exercise training where it is likely more pronounced.

It is not clear why specifically late exercise training leads to an increase in the abundance of SCFA-producing bacteria. One explanation may be fluctuations in lactate production at different times of day by active skeletal muscle and the subsequent uptake of lactate into the gut during exercise as previously

observed[51,52]. In the gut, lactate can directly be used as energy source and converted into SCFAs by gut bacteria[53-55]. While lactate production was not different during the morning and evening exercise in healthy volunteers[56], lactate levels were increased with late exercise training in mice[57] and the timing of exercise played a role in lactate production in patients with type 2 diabetes[58]. Additionally, the gut microbiota composition can itself oscillate, and in healthy conditions the abundance of *Lactobacillus*[59] and *Lachnospiraceae* [60] and other SCFA producers is increased near ZT22, when the late exercise training took place. Assuming the rhythmicity of the gut microbiota oscillation is somewhat maintained under the high-fat diet conditions in this study, it is possible that during the late exercise training the greater abundance of SCFA producers leads to an increased use of lactate or other metabolites as an energy source, which over time further promotes their proliferation and positive health changes. Acetate, the SCFAs produced in the highest quantities in the gut, is also instrumental for prolonged exercise endurance in mice[61], which corresponds to endurance being generally higher in the later part of the day[62].

To investigate the casual link between the altered microbiota and MASLD amelioration, we transplanted the microbiota of late-exercising into non-exercising mice. The findings from this experiment clearly support the role of the gut microbiota in later exercise-induced alleviation of liver steatosis. However, the MASLD amelioration was not as strong as in the exercising donor mice, for which there can be three explanations. Firstly, it is likely that the increased energy used by skeletal muscle during exercise substantially contributes to reduced liver lipid storage[63]. Secondly, a variable engraftment of the donor microbiota may have led to a division of recipients into 'low responders' with unimproved liver health and 'high responders' with ameliorated MASLD score and reduced liver TG content. This distinction appeared to be dependent on the engraftment success of the FMT, which has been proposed to play an important role in the positive FMT effects[64]. Thirdly, while RUN donors were trained for twelve weeks, their FMT recipient counterparts only received the microbiota transplantation for four weeks in total. This was owed to the assumption that changes to the gut microbiota composition in response to an intervention like exercise training take up to four weeks to be fully established in the donor mice[65]. An extension of the FMT period past the termination of the donors was not done due to the improved survival of fecal microbes during an FMT from fresh rather than frozen feces[66,67].

Overall, our findings show that only late, but not early exercise training is beneficial for the amelioration of steatosis in MASLD and that the associated changes to the composition of the gut microbiota likely play a causal role in this effect. Along with the improvement of liver steatosis with late exercise training, we observe an increase in beneficial bacterial taxa that are known to produce SCFAs, to compete for the use of dietary lipids, and generally improve health outcomes. This positive effect of late exercise training on the whole body and the liver was partially transferrable via a fecal microbiota transplantation, supporting the importance of a healthy gut-liver axis in the prevention and treatment of MASLD. Nonetheless, both early and late exercise trainings decreased inflammation in the liver. This suggests that any form of exercise is still preferable to sedentary behavior. While a multitude of additional factors such as chronotype, sleep quality and meal timing are to be considered for the optimal design of clinical lifestyle interventions, we here present the first proof that late exercise training may be a better treatment strategy than early exercise for the amelioration of MASLD.

Acknowledgement

The authors thank Milaine V. Hovingh, Jan Freark de Boer, Christiana Costa, Amanda Pronk, Salwa Afkir, Trea Streefland, Reshma Lalai, Chris van der Bent, Frank Otto, and Hetty Sips for their excellent technical assistance.

Author contribution: A.K., Z.Y., P.C.N.R and M.S. designed the experiments; A.K., Z.Y. S.Z., E.O., J.M.L., C.V. and M.S. collected and analyzed the data; A.K., Z.Y. and M.S. drafted the manuscript; B.G, Q.R.D. and P.C.N.R. critically revised the manuscript.

Supplementary information

Supplementary document 1: Supplementary figures 1-6

Supplementary document 2: Supplementary methods

Supplementary document 3: ImageJ scripts – can only be accessed online in the corresponding publication

References

1. Powell EE, Wong VW, Rinella M. Non-alcoholic fatty liver disease. *Lancet*. Jun 5 2021;397(10290):2212-2224. doi:10.1016/S0140-6736(20)32511-3
2. Rinella ME, Sookoian S. From NAFLD to MASLD: updated naming and diagnosis criteria for fatty liver disease. *J Lipid Res*. Jan 2024;65(1):100485. doi:10.1016/j.jlr.2023.100485
3. Loomba R, Friedman SL, Shulman GI. Mechanisms and disease consequences of nonalcoholic fatty liver disease. *Cell*. May 13 2021;184(10):2537-2564. doi:10.1016/j.cell.2021.04.015
4. Maestri M, Santopaolo F, Pompili M, Gasbarrini A, Ponziani FR. Gut microbiota modulation in patients with non-alcoholic fatty liver disease: Effects of current treatments and future strategies. *Front Nutr*. 2023;10:1110536. doi:10.3389/fnut.2023.1110536
5. Harrison SA, Bedossa P, Guy CD, et al. A Phase 3, Randomized, Controlled Trial of Resmetirom in NASH with Liver Fibrosis. *N Engl J Med*. Feb 8 2024;390(6):497-509. doi:10.1056/NEJMoa2309000
6. Houghton D, Stewart CJ, Day CP, Trenell M. Gut Microbiota and Lifestyle Interventions in NAFLD. *Int J Mol Sci*. Mar 25 2016;17(4):447. doi:10.3390/ijms17040447
7. Quante M, Mariani S, Weng J, et al. Zeitgebers and their association with rest-activity patterns. *Chronobiol Int*. Feb 1 2019;36(2):203-213. doi:10.1080/07420528.2018.1527347
8. Manella G, Sabath E, Aviram R, et al. The liver-clock coordinates rhythmicity of peripheral tissues in response to feeding. *Nat Metab*. Jun 2021;3(6):829-842. doi:10.1038/s42255-021-00395-7
9. Saran AR, Dave S, Zarrinpar A. Circadian Rhythms in the Pathogenesis and Treatment of Fatty Liver Disease. *Gastroenterology*. May 2020;158(7):1948-1966 e1. doi:10.1053/j.gastro.2020.01.050
10. Tahara Y, Shibata S. Entrainment of the mouse circadian clock: Effects of stress, exercise, and nutrition. *Free Radic Biol Med*. May 1 2018;119:129-138. doi:10.1016/j.freeradbiomed.2017.12.026
11. Bruns DR, Yusifova M, Marcello NA, Green CJ, Walker WJ, Schmitt EE. The Peripheral Circadian Clock and Exercise: Lessons from Young and Old Mice. *J Circadian Rhythms*. Dec 16 2020;18:7. doi:10.5334/jcr.201

12. Savikj M, Gabriel BM, Alm PS, et al. Afternoon exercise is more efficacious than morning exercise at improving blood glucose levels in individuals with type 2 diabetes: a randomised crossover trial. *Diabetologia*. Feb 2019;62(2):233-237. doi:10.1007/s00125-018-4767-z
13. van der Velde J, Boone SC, Winters-van Eekelen E, et al. Timing of physical activity in relation to liver fat content and insulin resistance. *Diabetologia*. Mar 2023;66(3):461-471. doi:10.1007/s00125-022-05813-3
14. Albalak G, Stijntjes M, van Bodegom D, et al. Setting your clock: associations between timing of objective physical activity and cardiovascular disease risk in the general population. *Eur J Prev Cardiol*. Feb 14 2023;30(3):232-240. doi:10.1093/eurjpc/zwac239
15. Schonke M, Ying Z, Kovynev A, et al. Time to run: Late rather than early exercise training in mice remodels the gut microbiome and reduces atherosclerosis development. *FASEB J*. Jan 2023;37(1):e22719. doi:10.1096/fj.202201304R
16. Kovynev A, Ying Z, Lambooij JM, et al. Early but Not Late Exercise Training in Mice Exacerbates Hepatic Inflammation in Developing Nonalcoholic Fatty Liver Disease. *J Clin Transl Hepatol*. Oct 28 2023;11(5):1282-1285. doi:10.14218/JCTH.2023.00094
17. Hsu CL, Schnabl B. The gut-liver axis and gut microbiota in health and liver disease. *Nat Rev Microbiol*. Nov 2023;21(11):719-733. doi:10.1038/s41579-023-00904-3
18. Malesza IJ, Malesza M, Walkowiak J, et al. High-Fat, Western-Style Diet, Systemic Inflammation, and Gut Microbiota: A Narrative Review. *Cells-Basel*. Nov 2021;10(11)doi:10.3390/cells10113164
19. Kim KA, Gu W, Lee IA, Joh EH, Kim DH. High Fat Diet-Induced Gut Microbiota Exacerbates Inflammation and Obesity in Mice via the TLR4 Signaling Pathway. *Plos One*. Oct 16 2012;7(10)doi:10.1371/journal.pone.0047713
20. Liu C, Schönke M, Spoorenberg B, et al. FGF21 protects against hepatic lipotoxicity and macrophage activation to attenuate fibrogenesis in nonalcoholic steatohepatitis. *Elife*. Jan 17 2023;12doi:10.7554/eLife.83075
21. Westerterp M, van der Hoogt CC, de Haan W, et al. Cholesteryl ester transfer protein decreases high-density lipoprotein and severely aggravates atherosclerosis in APOE*3-Leiden mice. *Arterioscler Thromb Vasc Biol*. Nov 2006;26(11):2552-9. doi:10.1161/01.ATV.0000243925.65265.3c

22. van Eenige R, Verhave PS, Koemans PJ, Tiebosch I, Rensen PCN, Kooijman S. RandoMice, a novel, user-friendly randomization tool in animal research. *PLoS One*. 2020;15(8):e0237096. doi:10.1371/journal.pone.0237096
23. du Sert NP, Hurst V, Ahluwalia A, et al. The ARRIVE guidelines 2.0: Updated guidelines for reporting animal research. *Plos Biol*. Jul 2020;18(7)doi:10.1371/journal.pbio.3000410
24. Parthasarathy G, Revelo X, Malhi H. Pathogenesis of Nonalcoholic Steatohepatitis: An Overview. *Hepatol Commun*. Apr 2020;4(4):478-492. doi:10.1002/hep4.1479
25. Dalbram E, Basse AL, Zierath JR, Treebak JT. Voluntary wheel running in the late dark phase ameliorates diet-induced obesity in mice without altering insulin action. *J Appl Physiol*. Apr 2019;126(4):993-1005. doi:10.1152/japplphysiol.00737.2018
26. Hsu CC, Ness E, Kowdley KV. Nutritional Approaches to Achieve Weight Loss in Nonalcoholic Fatty Liver Disease. *Adv Nutr*. Mar 2017;8(2):253-265. doi:10.3945/an.116.013730
27. Kohsaka A, Laposky AD, Ramsey KM, et al. High-fat diet disrupts behavioral and molecular circadian rhythms in mice. *Cell Metabolism*. Nov 2007;6(5):414-421. doi:10.1016/j.cmet.2007.09.006
28. van Moorsel D, Hansen J, Havekes B, et al. Demonstration of a day-night rhythm in human skeletal muscle oxidative capacity. *Mol Metab*. Aug 2016;5(8):635-645. doi:10.1016/j.molmet.2016.06.012
29. Winget CM, DeRoshia CW, Holley DC. Circadian rhythms and athletic performance. *Med Sci Sports Exerc*. Oct 1985;17(5):498-516.
30. Segers A, Desmet L, Thijs T, Verbeke K, Tack J, Depoortere I. The circadian clock regulates the diurnal levels of microbial short-chain fatty acids and their rhythmic effects on colon contractility in mice. *Acta Physiol*. Mar 2019;225(3)doi:10.1111/apha.13193
31. Henagan TM, Stefanska B, Fang ZD, et al. Sodium butyrate epigenetically modulates high-fat diet-induced skeletal muscle mitochondrial adaptation, obesity and insulin resistance through nucleosome positioning. *Brit J Pharmacol*. Jun 2015;172(11):2782-2798. doi:10.1111/bph.13058
32. Pan JH, Kim JH, Kim HM, et al. Acetic acid enhances endurance capacity of exercise-trained mice by increasing skeletal muscle oxidative properties. *Biosci Biotech Bioch*. Sep 2 2015;79(9):1535-1541. doi:10.1080/09168451.2015.1034652

33. Ioannou GN. The Role of Cholesterol in the Pathogenesis of NASH. *Trends Endocrin Met*. Feb 2016;27(2):84-95. doi:10.1016/j.tem.2015.11.008
34. Houttu V, Boulund U, Grefhorst A, et al. The role of the gut microbiome and exercise in non-alcoholic fatty liver disease. *Therap Adv Gastroenterol*. 2020;13:1756284820941745. doi:10.1177/1756284820941745
35. Kamer O, Rinott E, Tsaban G, et al. Successful weight regain attenuation by autologous fecal microbiota transplantation is associated with non-core gut microbiota changes during weight loss; randomized controlled trial. *Gut Microbes*. Dec 18 2023;15(2)doi:10.1080/19490976.2023.2264457
36. Shephard RJ, Allen C, Benade AJ, et al. The maximum oxygen intake. An international reference standard of cardiorespiratory fitness. *Bull World Health Organ*. 1968;38(5):757-64.
37. Durk RP, Castillo E, Márquez-Magaña L, et al. Gut Microbiota Composition Is Related to Cardiorespiratory Fitness in Healthy Young Adults. *Int J Sport Nutr Exe*. May 2019;29(3):249-253. doi:10.1123/ijsnem.2018-0024
38. Hughes RL. A Review of the Role of the Gut Microbiome in Personalized Sports Nutrition. *Front Nutr*. Jan 10 2020;6doi:10.3389/fnut.2019.00191
39. Hasani A, Ebrahimzadeh S, Hemmati F, Khabbaz A, Hasani A, Gholizadeh P. The role of Akkermansia muciniphila in obesity, diabetes and atherosclerosis. *J Med Microbiol*. 2021;70(10)doi:10.1099/jmm.0.001435
40. Li J, Lin SQ, Vanhoutte PM, Woo CW, Xu AM. Akkermansia Muciniphila Protects Against Atherosclerosis by Preventing Metabolic Endotoxemia-Induced Inflammation in Apoe-/- Mice. *Circulation*. Jun 14 2016;133(24):2434-+. doi:10.1161/Circulationaha.115.019645
41. Depommier C, Van Hul M, Everard A, Delzenne NM, De Vos WM, Cani PD. Pasteurized Akkermansia muciniphila increases whole-body energy expenditure and fecal energy excretion in diet-induced obese mice. *Gut Microbes*. 2020;11(5):1231-1245. doi:10.1080/19490976.2020.1737307
42. Plovier H, Everard A, Druart C, et al. A purified membrane protein from Akkermansia muciniphila or the pasteurized bacterium improves metabolism in obese and diabetic mice. *Nat Med*. Jan 2017;23(1):107-113. doi:10.1038/nm.4236
43. Lee NY, Shin MJ, Youn GS, et al. Lactobacillus attenuates progression of nonalcoholic fatty liver disease by lowering cholesterol and steatosis. *Clin Mol Hepatol*. Jan 2021;27(1):110-124. doi:10.3350/cmh.2020.0125

44. Li HZ, Liu F, Lu JJ, et al. Probiotic Mixture of Lactobacillus plantarum Strains Improves Lipid Metabolism and Gut Microbiota Structure in High Fat Diet-Fed Mice. *Front Microbiol*. Mar 26 2020;11doi:10.3389/fmicb.2020.00512
45. Jang HR, Park HJ, Kang D, et al. A protective mechanism of probiotic Lactobacillus against hepatic steatosis via reducing host intestinal fatty acid absorption. *Exp Mol Med*. Aug 13 2019;51doi:10.1038/s12276-019-0293-4
46. Guo WL, Xiang QR, Mao BY, et al. Protective Effects of Microbiome-Derived Inosine on Lipopolysaccharide-Induced Acute Liver Damage and Inflammation in Mice via Mediating the TLR4/NF-κB Pathway. *J Agr Food Chem*. Jul 14 2021;69(27):7619-7628. doi:10.1021/acs.jafc.1c01781
47. Li Z, Yi CX, Katiraei S, et al. Butyrate reduces appetite and activates brown adipose tissue via the gut-brain neural circuit. *Gut*. Jul 2018;67(7):1269-1279. doi:10.1136/gutjnl-2017-314050
48. Deng MJ, Qu F, Chen L, et al. SCFAs alleviated steatosis and inflammation in mice with NASH induced by MCD. *J Endocrinol*. Jun 2020;245(3):425-437. doi:10.1530/Joe-20-0018
49. Martin-Gallausiaux C, Marinelli L, Blottière HM, Larraufie P, Lapaque N. SCFA: mechanisms and functional importance in the gut. *P Nutr Soc*. Feb 2021;80(1):37-49. doi:10.1017/S0029665120006916
50. Frampton J, Murphy KG, Frost G, Chambers ES. Short-chain fatty acids as potential regulators of skeletal muscle metabolism and function. *Nat Metab*. Sep 2020;2(9):840-848. doi:10.1038/s42255-020-0188-7
51. Smith KA, Pugh JN, Duca FA, Close GL, Ormsbee MJ. Gastrointestinal pathophysiology during endurance exercise: endocrine, microbiome, and nutritional influences. *Eur J Appl Physiol*. Oct 2021;121(10):2657-2674. doi:10.1007/s00421-021-04737-x
52. Scheiman J, Luber JM, Chavkin TA, et al. Meta-omics analysis of elite athletes identifies a performance-enhancing microbe that functions via lactate metabolism. *Nat Med*. Jul 2019;25(7):1104-+. doi:10.1038/s41591-019-0485-4
53. Belenguer A, Holtrop G, Duncan SH, et al. Rates of production and utilization of lactate by microbial communities from the human colon. *Fems Microbiol Ecol*. Jul 2011;77(1):107-119. doi:10.1111/j.1574-6941.2011.01086.x
54. Louis P, Flint HJ. Diversity, metabolism and microbial ecology of butyrate-producing bacteria from the human large intestine. *Fems Microbiol Lett*. May 2009;294(1):1-8. doi:10.1111/j.1574-6968.2009.01514.x

55. Wang SP, Rubio LA, Duncan SH, et al. Pivotal Roles for pH, Lactate, and Lactate-Utilizing Bacteria in the Stability of a Human Colonic Microbial Ecosystem. *Msystems*. Sep-Oct 2020;5(5)doi:10.1128/mSystems.00645-20
56. Sekir U, Ozyener F, Gur H. Effect of time of day on the relationship between lactate and ventilatory thresholds: a brief report. *J Sports Sci Med*. Dec 2002;1(4):136-40.
57. Casanova-Vallve N, Duglan D, Vaughan ME, et al. Daily running enhances molecular and physiological circadian rhythms in skeletal muscle. *Mol Metab*. Jul 2022;61doi:10.1016/j.molmet.2022.101504
58. Heden TD, Liu Y, Kanaley JA. Exercise timing and blood lactate concentrations in individuals with type 2 diabetes. *Appl Physiol Nutr Me*. Jul 2017;42(7):732-737. doi:10.1139/apnm-2016-0382
59. Thaiss CA, Levy M, Korem T, et al. Microbiota Diurnal Rhythmicity Programs Host Transcriptome Oscillations. *Cell*. Dec 1 2016;167(6):1495-1510 e12. doi:10.1016/j.cell.2016.11.003
60. Heddes M, Altaha B, Niu Y, et al. The intestinal clock drives the microbiome to maintain gastrointestinal homeostasis. *Nat Commun*. Oct 14 2022;13(1):6068. doi:10.1038/s41467-022-33609-x
61. Okamoto T, Morino K, Ugi S, et al. Microbiome potentiates endurance exercise through intestinal acetate production. *Am J Physiol-Endoc M*. May 2019;316(5):E956-E966. doi:10.1152/ajpendo.00510.2018
62. Kang J, Ratamess NA, Faigenbaum AD, et al. Time-of-Day Effects of Exercise on Cardiorespiratory Responses and Endurance Performance-A Systematic Review and Meta-Analysis. *J Strength Cond Res*. Oct 2023;37(10):2080-2090. doi:10.1519/Jsc.0000000000004497
63. Xue YQ, Peng Y, Zhang LT, Ba Y, Jin G, Liu G. Effect of different exercise modalities on nonalcoholic fatty liver disease: a systematic review and network meta-analysis. *Sci Rep-Uk*. Mar 14 2024;14(1)doi:10.1038/s41598-024-51470-4
64. Porcari S, Benech N, Valles-Colomer M, et al. Key determinants of success in fecal microbiota transplantation: From microbiome to clinic. *Cell Host Microbe*. May 10 2023;31(5):712-733. doi:10.1016/j.chom.2023.03.020
65. Liu ZH, Liu HY, Zhou HB, et al. Moderate-Intensity Exercise Affects Gut Microbiome Composition and Influences Cardiac Function in Myocardial Infarction Mice. *Front Microbiol*. Sep 1 2017;8doi:10.3389/fmicb.2017.01687
66. Bilinski J, Dziurzynski M, Grzesiowski P, et al. Fresh Versus Frozen Stool for Fecal Microbiota Transplantation-Assessment by Multimethod Approach

Combining Culturing, Flow Cytometry, and Next-Generation Sequencing. *Front Microbiol*. Jul 1 2022;13doi:10.3389/fmicb.2022.872735
67. Liu JL, Lin H, Cao M, et al. Shifts and importance of viable bacteria in treatment of DSS-induced ulcerative colitis mice with FMT. *Front Cell Infect Mi*. Feb 6 2023;13doi:10.3389/fcimb.2023.1124256

Supplementary figures

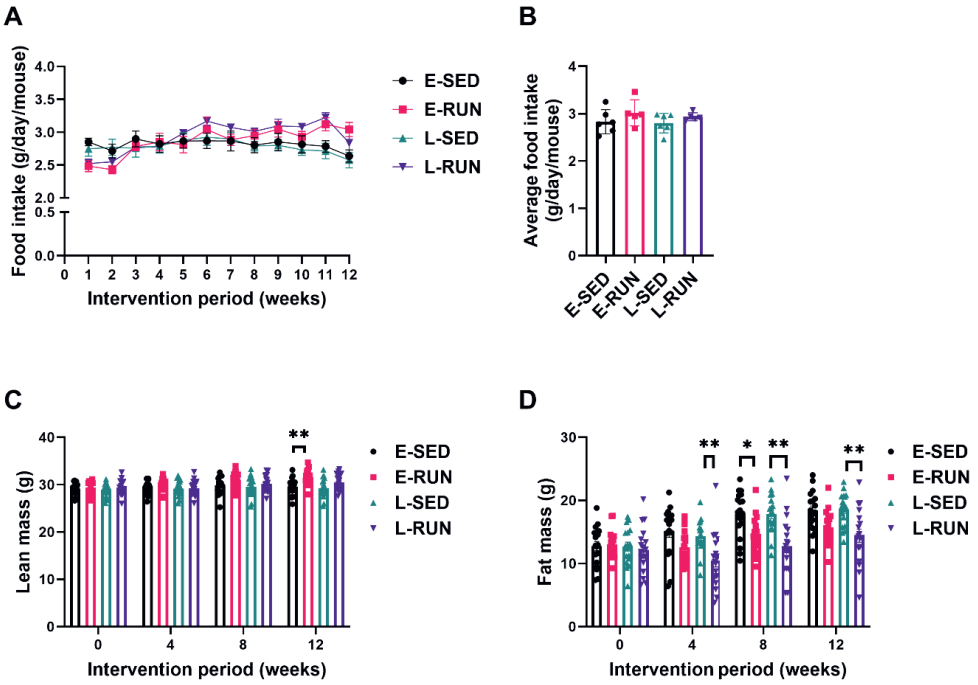

Supplementary figure 1. Effect of timed exercise training on food intake, lean and fat mass over time. (**A**) Daily food intake throughout the study and (**B**) average daily food intake were assessed per cage and divided by the number of mice per cage. (**C**) Lean mass and (**D**) fat mass were measured every four weeks. Data are presented as mean ± SEM (n = 4-5 cages for **A** and **B**, and n = 16–18 for **C** and **D**), *p < 0.05, **p < 0.01, ***p < 0 .001 according to two-way ANOVA with post-hoc Tukey test for multiple comparisons.

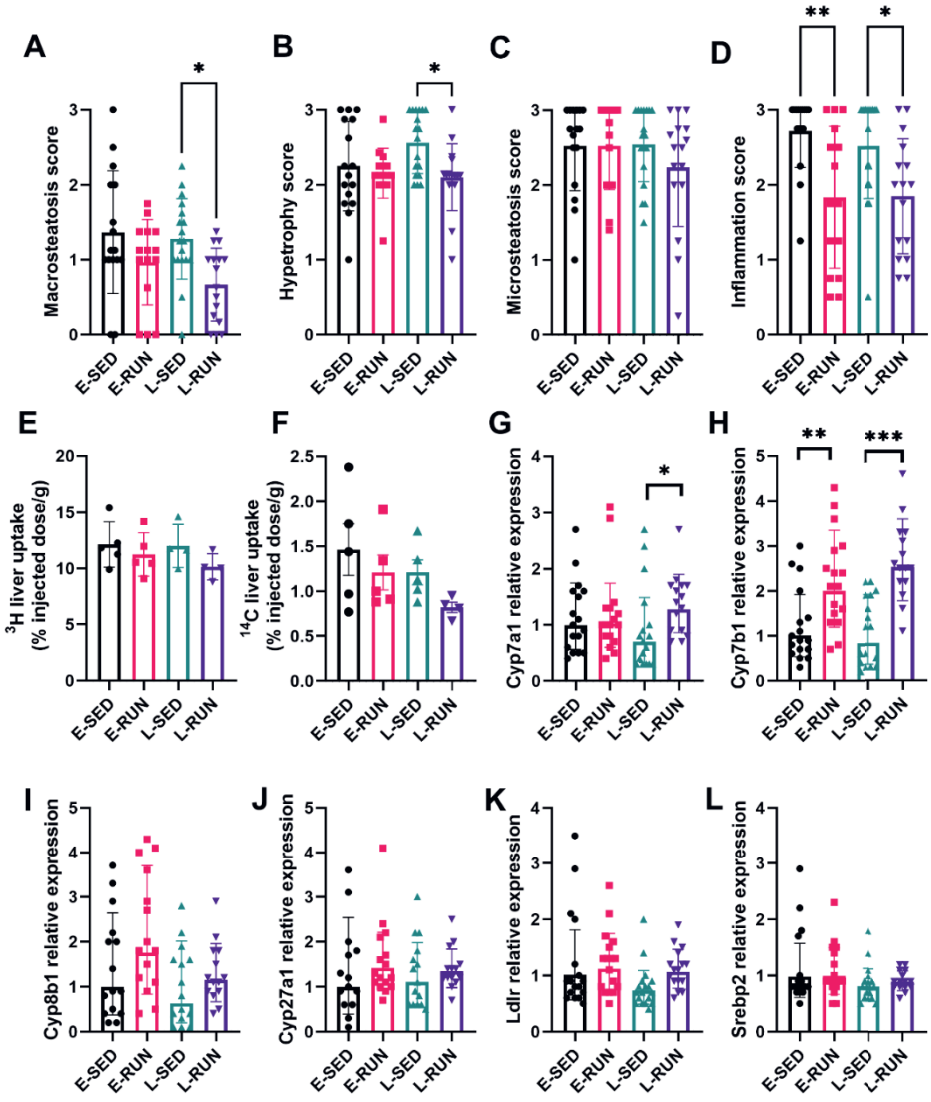

Supplementary figure 2. Effect of timed exercise training on the liver steatosis, particles uptake and gene expression. With H&E staining, individual (**A**) macrosteatosis, (**B**) hypertrophy, (**C**) microsteatosis and (**D**) inflammation scores were assessed. To better assess liver function, the uptake of (**E**) glycerol tri[^{3}H]oleate and (**F**) [^{14}C]deoxyglucose was quantified. The relative expression of (**G**) *Ldlr*, (**H**) *Cyp27a1*, (**I**) *Cyp7a1*, (**J**) *Cyp8b1*, (**K**) *Srebp2* and (**L**) *Cyp7b1* genes was measured with RT-qPCR. Data are presented as mean ± SEM (n = 16–18 for A-D, n = 4–5 for E

and F), and as geometric mean ± geometric SD (n = 16–18) for G-L, *p < 0.05, **p < 0.01 according to one-way ANOVA with Tukey multiple comparison test.

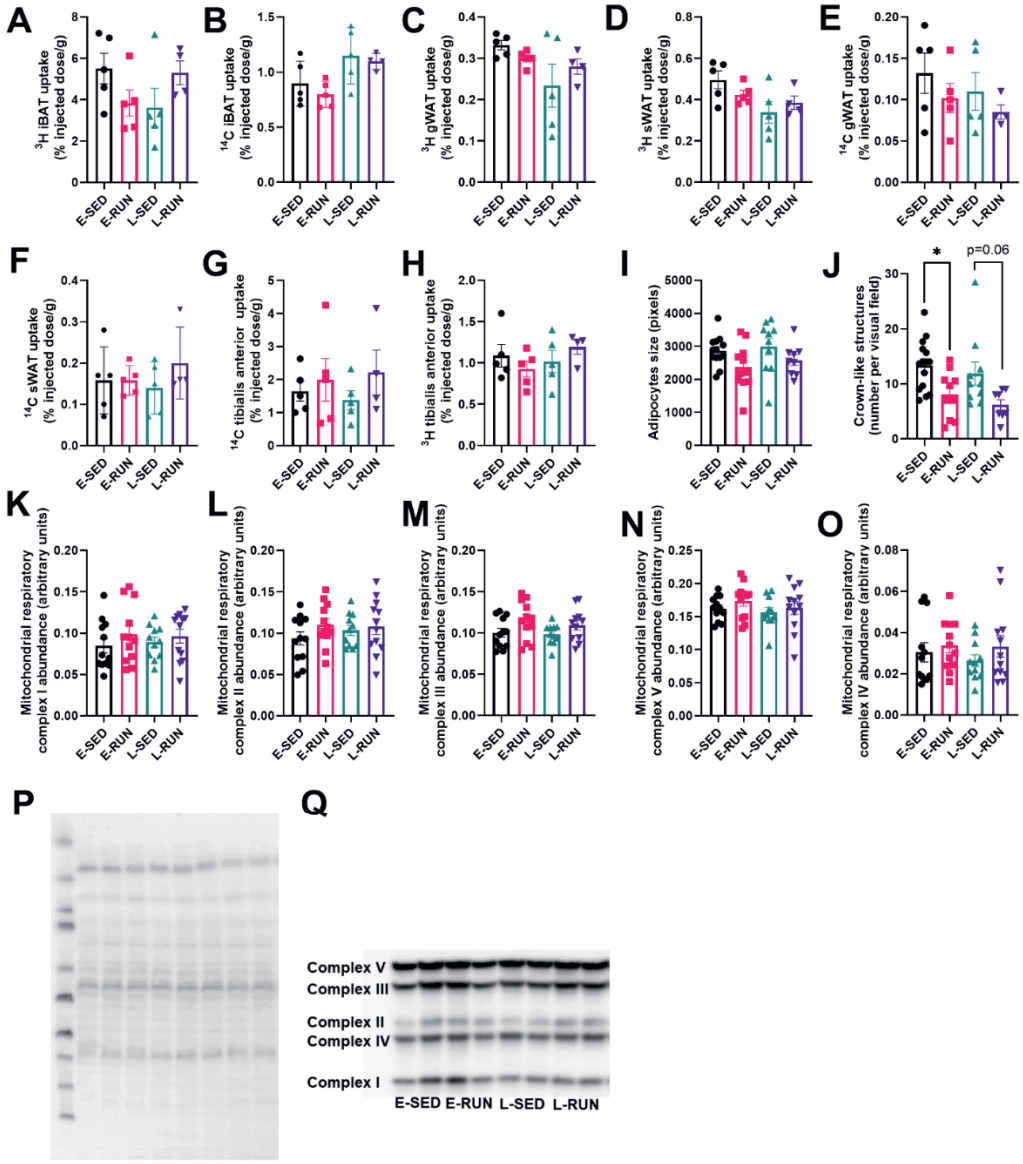

Supplementary figure 3. Effect of timed exercise training on adipose tissue and skeletal muscle (Tibialis anterior). To assess adipose tissue function, the uptake of glycerol tri[^{3}H]oleate and [^{14}C]deoxyglucose was quantified in (**A,B**) iBAT, (**C,D**)

gWAT, (**E,F**) sWAT and (**G,H**) tibalis anterior. With H&E staining, the (**I**) adipocyte size and (**K**) the amount of crown-like structures were quantified. To quantify changes in skeletal muscle oxidative capacity, (**K-O**) the abundance of mitochondrial respiratory complexes I-V was measured with Western blots, (**P-Q**) normalized to the total protein content on Ponceau S staining. Data are presented as mean ± SEM (with n = 4-5 for **A-G** and **I,J**; n=10-13 for **G** and **H**, and n=8 for **K-O**), *p < 0.05, **p < 0.01 according to one-way ANOVA with Tukey multiple comparison test.

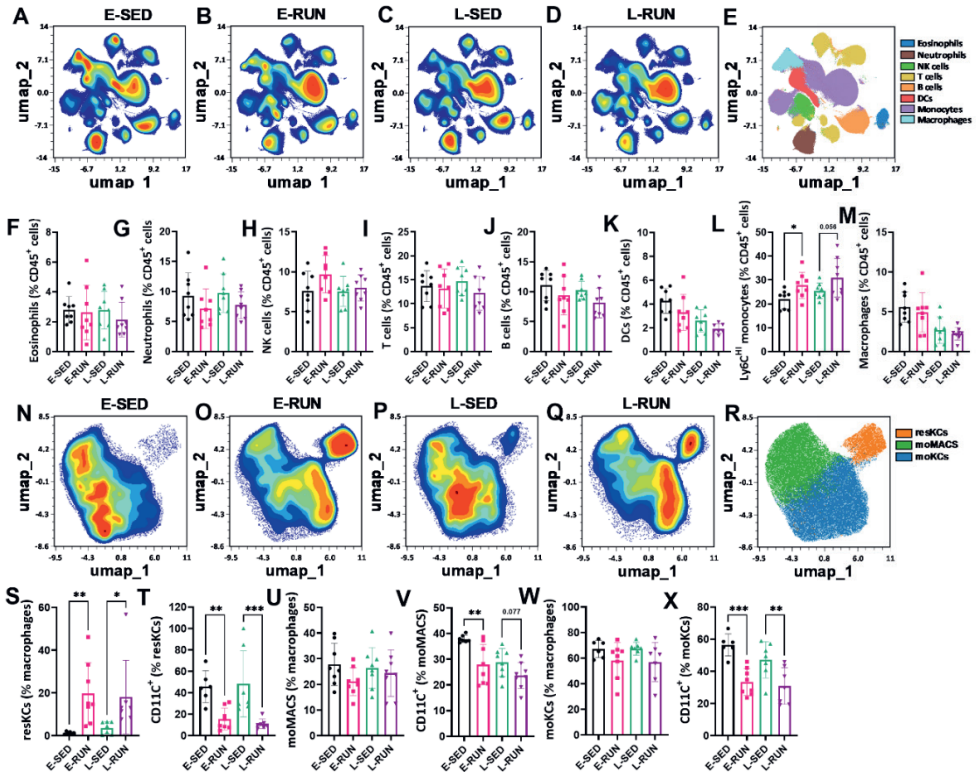

Supplementary figure 4. Effect of timed exercise training on the immune cell composition in the liver. Isolated hepatic immune cells were analyzed using spectral flow cytometry. **A-E** Show uniform manifold approximation and projection for dimension reduction of the total hepatic immune cell composition and **N-R** for the different macrophage subsets. Changes in (**F**) Eosonophils, (**G**) Neutrophils, (**H**) NK cells, (**I**) T cells, (**J**) B cells, (**K**) dendritic cells, (**L**) Ly6c^{HI} monocytes and (**M**) macrophages are shown, as well as the changes in (**S**) resKCs (resident Kupffer cells)

as % of macrophages, (**T**) $CD11C^+$ cells as % of resKCs, (**U**) moMACS (monocyte-derived macrophages) as % of all macrophages, (**V**) $CD11C^+$ cells as % of moMACS, (**W**) moKCs as % of macrophages and (**X**) $CD11C^+$ cells as % of moKCs (monocyte-derived Kupffer cells). Data are presented as mean ± SEM (n = 8), *$p < 0.05$, **$p < 0.01$ according to one-way ANOVA with post-hoc Tukey test for multiple comparisons.

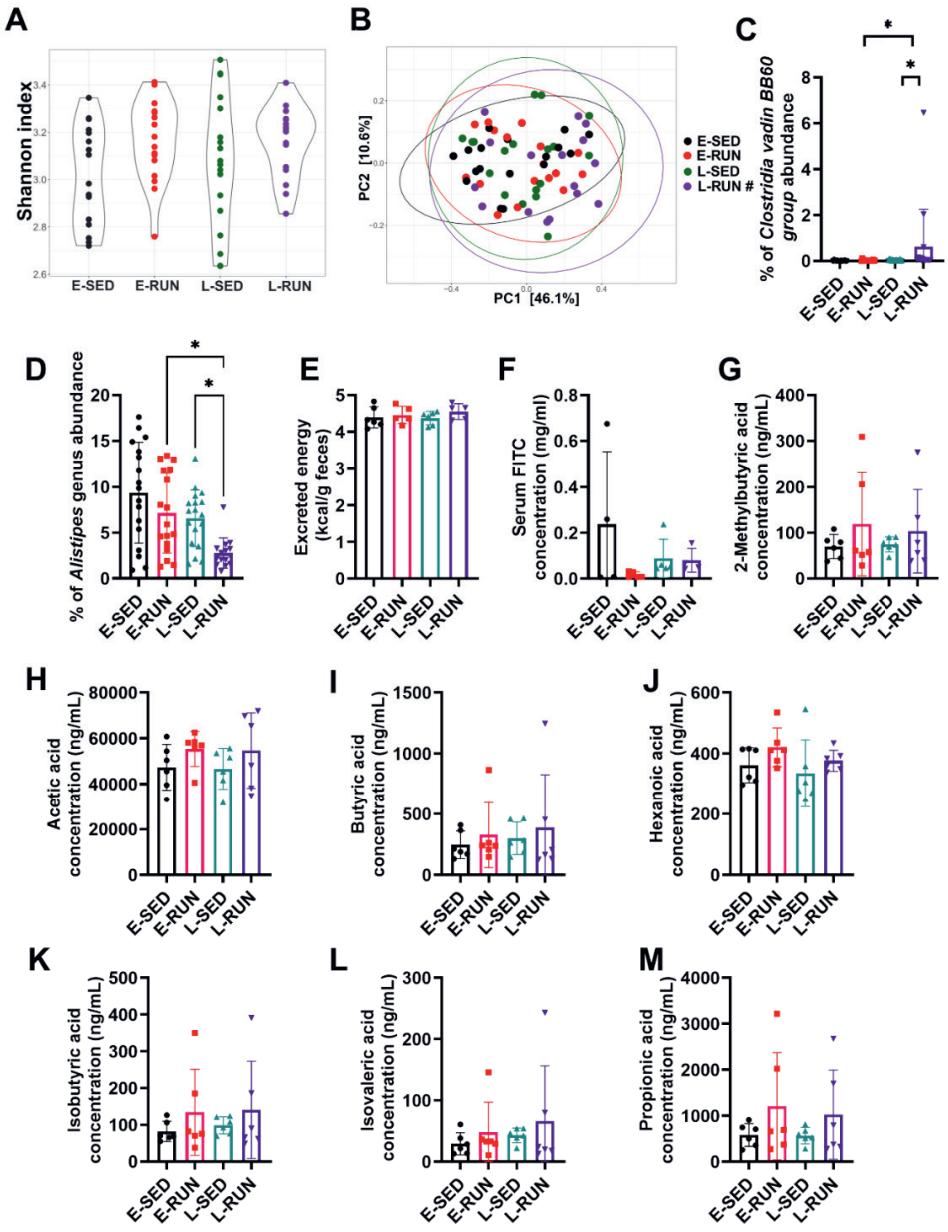

Supplementary figure 5. Effect of timed exercise training on the gut and portal vein changes. 16S sequencing was conducted on all cecum content samples and (**A**) α-diversity and (**B**) β-diversity were calculated. (**C**) *Clostridia vadin BB60 group* family was increased in L-RUN compared to other groups, while (**D**) abundance of *Alistipes* genus was decreased. To further investigate the impact of gut microbiota

on the body, (**E**) changes in the feces caloric output were quantified, (**F**) intestinal permeability was measured with FITC-Dextran, and the (**G**) concentration of 2-methylbutyric, (**H**) acetic, (**I**) butyric, (**J**) hexanoinc, (**K**) isobutyric, (**L**) isovaleric and (**M**) propionic short-chain fatty acids was quantified in portal vein blood plasma. One-way ANOVA with Tukey post-hoc test for multiple comparisons (n=16-18) was used in **A**, PERMANOVA with Bonferroni correction was used in **B,** with # showing comparison between L-SED and L-RUN, where # stands for $p<0.05$, Wald test with FDR set to 0.05 was used for **C**, **D**, with * $p<0.05$, Data in **E-M** are presented as mean ± SEM (n = 4-6), according to one-way ANOVA with Tukey multiple comparison test.

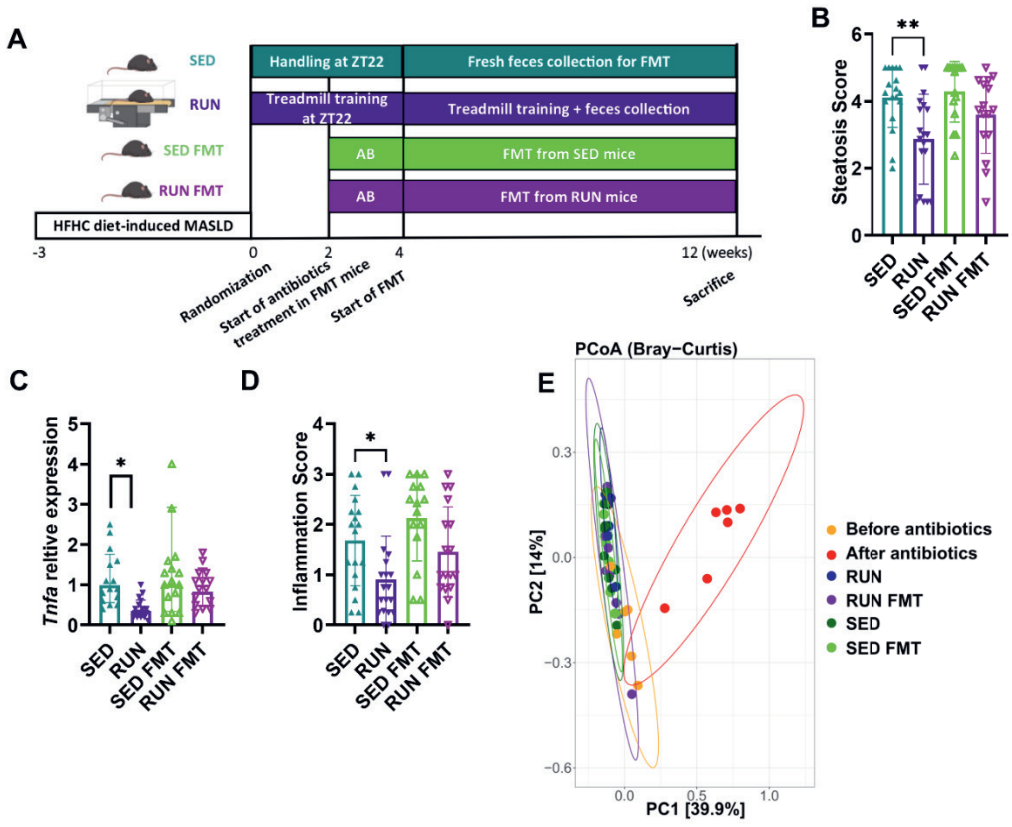

Supplementary figure 6. Effect of exercise-to-sedentary and sedentary-to-sedentary FMT on the liver and gut. (**A**) timeline of animal experiment 2, in which mice were transplanted with the fecal microbiota of sedentary or exercising mice. We studied the effect of transplantation on (**B**) steatosis score, (**C**) *Tnfa* gene expression and (**D**) inflammatory score as well as on (**E**) the changes in the gut β-diversity. Data is presented as mean ± SEM (n = 18-20) for **B** and **D** and as geometric mean ± geometric SD (n=16-18) for **C** with * p<0.05, according to one-way ANOVA with Tukey test for multiple comparisons. PERMANOVA with Bonferroni correction was used to investigate the differences in β-diversity between the groups in **E**.

Supplementary methods

Sample-size estimation

To calculate the required number of mice, a power calculation was performed for a one-way anova with 4 multiple comparisons. Based on the rodent NAFLD scoring system (Liang et al., doi: 10.1371/journal.pone.0115922), we find a difference of 25% between groups biologically relevant. Based on previous studies with this mouse line we expected a relatively large variability in hepatic fat accumulation and inflammation between animals, namely SD=22%. To detect this difference between the groups with an alpha = 5% and a Power = 80% in 4 pairwise comparisons we needed n = 18 mice per group.

Blinding

Due to the nature of the experiment, groups were not blinded during the animal study. For the further analysis, all histological images were blinded before the analysis. During other measurements, researchers were not aware which sample belonged to which group, and the order of samples was mixed, excluding the chance for the batch effect between the groups.

Humane endpoints

For the first experiment, weight loss of 10 percent, or the inability to rise or ambulate, or the oral gavage complications, such as labored breathing, signs of swelling around the head or front legs and bleeding from mouth or nose were defined as the humane endpoints, upon reaching which, the mice would have been euthanized. In the second experiment, due to antibiotics use, the weight loss endpoint was changed to weight loss of 15% in one week or loss of 20% of bodyweight throughout the study, and longer than 3 days diarrhea was added as another humane endpoint.

Animals also were removed from the treadmill with signs of exhaustion (i.e. the lack of attempts to get back on the treadmill belt despite being nudged) and monitored until their recovery.

Exercise training protocol

Mice were trained on a rat treadmill with five lanes (MazeEngineers, Skokie, Illinois, USA), allowing two to four cage mates to run together per lane, as previously

described[1], with minor adjustments. Briefly, in experiment 1, after three days of treadmill acclimatization with gradually increasing duration and speed, mice were trained for one hour per day, on five consecutive days per week for 12 weeks beginning with 15 minutes at 6-14 m/min followed by 45 minutes at 15 m/min. After two weeks of training, the maximum speed was increased from 15 to 17 m/min for both training groups until week eight when the speed was decreased back to 15 m/min for both groups as mice struggled to keep running at 17 m/min due to increased body weight. This speed corresponds to a moderate effort exercise. The speed was adjusted throughout the study to ensure that all mice were able to finish the training bouts so that all mice received the same training load. In experiment 2, mice followed a similar exercise protocol, though with a maximum speed of 17 m/min throughout the whole study. The exercise training took place under dim red light illumination during the dark phase at either ZT13 or ZT22.

Antibiotic treatment

Recipient mice were given 200 µL of antibiotic cocktail (0.5 mg/mL ampicillin, 0.5 mg/mL neomycin, 0.5 mg/mL metronidazole, and 0.25 mg/mL vancomycin) by oral gavage for two days at ZT0. Four mice developed colitis in response and had to be excluded from the study. Thereafter, the rest of the mice were switched to receive antibiotics via the drinking water (0.25 mg/mL ampicillin, 0.25 mg/mL neomycin, 0.25 mg/mL metronidazole, and 0.125 mg/mL vancomycin) for another 12 days which was tolerated well.

Fecal microbiota transplantation

Fresh feces were collected from RUN and SED donors during the first ten minutes of treadmill training via a tray under the treadmill or by placing the mice into clean empty cages without bedding, respectively. The feces were pooled and immediately homogenized in Ringer's solution supplemented with 0.05% L-cysteine hydrochloride (Ringers solution 1/4 strength tablets, NutriSelect Basic, 96724, Darmstadt, Germany). The fecal slurry was filtered through a 100 µm cell strainer, vortexed and centrifuged at 200 RCF for 5 min at 4°C, and 200 µL of the fecal bacteria suspension per mouse was orally administrated to the recipient mice from the corresponding recipient group per gavage.

Body weight, body composition and food intake assessment

Body weight of the mice and food intake per cage were assessed weekly at approximately ZT0. Every four weeks, body fat and lean mass were measured by EchoMRI 100-Analyzer (EchoMRI, Houston, Texas, USA).

Plasma lipid and glucose measurements

Every four weeks, tail vein blood was collected into paraoxon-coated glass capillaries, and plasma was obtained after centrifugation for 5 min at 11,200 RCF and 4°C. Plasma TG and TC were measured using commercial enzymatic kits (10166588130 and 11489232216, respectively, Roche Diagnostics, Mannheim, Germany) as recommended by the manufacturer. Plasma glucose concentration was measured during the blood draw with a glucosemeter (Accu-Check, Roche, Basel, Switzerland).

Intestinal permeability measurement

In experiment 1, three hours into fasting on the day of sacrifice, mice (n=5 per group) received 150 µL of FITC-Dextran (0.6 mg/g body weight; 46944, Sigma-Aldrich, St. Louis, Missouri, USA; dissolved in water) via oral gavage. One hour later, mice were sacrificed, and heart puncture blood was collected into serum separator clot activator tubes (BD Vacutainer tube SST II 5ml yellow, 367953, Becton Dickinson, Vianen, the Netherlands). Serum was then diluted 1:5 in cold PBS and fluorescence intensity was measured spectrophotometrically (λ_{ex} 485 nm and λ_{em} 535 nm) in a fluorescent microplate reader (GloMax Discover, Promega, Madison, Wisconsin, USA) in black-wall 96-well plates.

Liver immune cell isolation and flow cytometry

In experiment 1, isolation of liver leukocytes (n=8 per group) was performed as previously described [2]. Briefly, liver tissue was collected in ice-cold RPMI1640+ Glutamax (Gibco, Waltham, Massachusetts, USA) and subsequently minced and digested for 25 min at 37°C under agitation (40 RCF) in RPMI1640+Glutamax supplemented with 1 mg/mL collagenase type IV from *Clostridium histolyticum* (Sigma-Aldrich, St. Louis, Missouri, USA), 1 mg/mL Dispase II (Sigma-Aldrich, St. Louis, Missouri, USA), 1 mg/mL Collagenase D from *C. histoloyticum* (Sigma-Aldrich, St. Louis, Missouri, USA) and 2000 U/mL DNase I (Sigma-Aldrich, St. Louis, Missouri, USA). After digestion, samples were passed through a 100 µm cell strainer, pelleted

at 300 RCF for 10 min at 4°C and washed twice with PBS supplemented with 1% heat-inactivated fetal calf serum (hiFCS; Serana GmbH, Pessin, Germany) and 2.5 mM EDTA (Sigma-Aldrich, St. Louis, Missouri, USA). After washing, the pellets were treated with 3 mL erythrocyte lysis buffer consisting of 0.15 M NH_4Cl (Merck, Rahway, New Jersey, USA), 1 mM $KHCO_3$ (Merck, Rahway, New Jersey, USA) and 0.1 mM EDTA in ddH_2O for 2 minutes. Next, leukocytes were isolated by means of magnetic-activated cell sorting using LS columns and CD45 MicroBeads (Miltenyi Biotec, Bergisch Gladbach, Germany) according to the manufacturer's protocol. Total isolated $CD45^+$ cells were counted and stained with Zombie NIR (Biolegend, San Diego, California, USA) followed by fixation with 1.9% paraformaldehyde (Sigma-Aldrich, St. Louis, Missouri, USA).

Post-fixation, the samples were incubated for 30 minutes at 4°C with a the cocktail of antibodies (Table 1) in PBS/FCS/EDTA supplemented with Brilliant stain buffer plus (BD Biosciences, Franklin Lakes, New Jersey, USA) and True-stain monocyte blocker (Biolegend, San Diego, California, USA).

The stained samples were subsequently measured using a 3-laser Cytek Aurora spectral flow cytometer (Cytek Biosciences, Fremont, CA, USA). Spectral unmixing of the acquired data was performed using SpectroFlow v3.0 (Cytek Biosciences), gating was performed using FlowJo™ v10.8 (BD Biosciences, Franklin Lakes, NJ, USA) and UMAPs were generated using OMIQ (Dotmatics, Boston, MA, USA).

Flow cytometry gating strategy

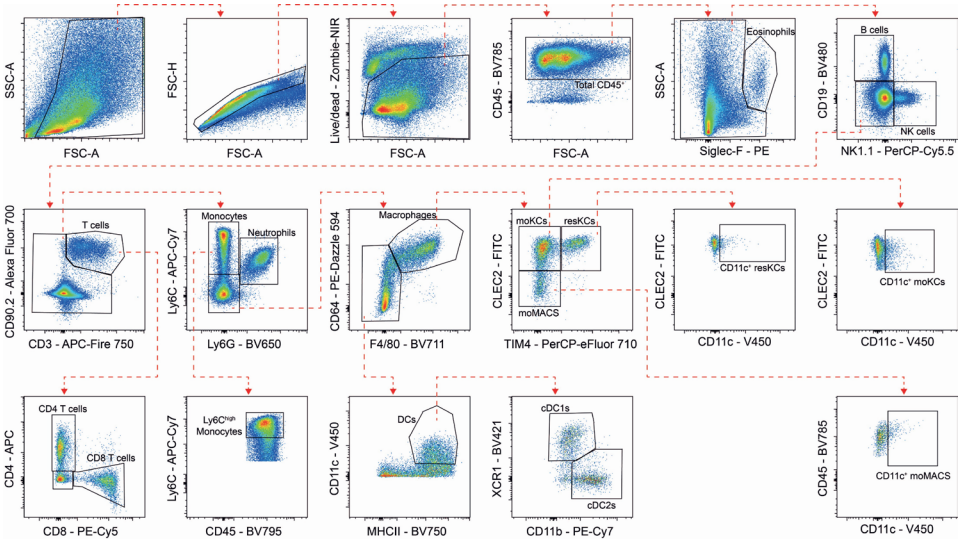

Table 1. Antibodies used for flow cytometry

Target	Clone	Conjugate	Source	Catalog no.	RRID
CD3	17A2	APC/Fire-810	Biolegend	100267	AB_2876392
CD4	RM4-5	APC	eBioscience	17-0042-82	AB_469323
CD8	53-6.7	PE-Cy5	Invitrogen	35-0081-82	AB_11217674
CD11b	M1/70	PE-Cy7	eBioscience	25-0112-82	AB_469588
CD11c	B-ly6	V450	BD Biosciences	560370	AB_1645557
CD19	1D3	BV480	BD Biosciences	566107	AB_2739509
CD45	30-F11	BV785	Biolegend	103149	AB_2564590
CD64	X54-5/7.1	PE-Dazzle 594	Biolegend	139320	AB_2566559
CD90.2	30-H12	Alexa Fluor 700	Biolegend	105320	AB_493725
CLEC2	17D9	FITC	Bio-Rad	MCA5700	AB_11152776
F4/80	BM8	BV711	Biolegend	123147	AB_2564588
Ly6C	HK1.4	APC-Cy7	Biolegend	128025	AB_10643867
Ly6G	1A8	BV650	Biolegend	127641	AB_2565881
MHCII	2G9	BV750	BD Biosciences	747317	AB_2872025
NK1.1	PK136	PerCP-Cy5.5	Biolegend	108727	AB_2132706
TIM4	RMT4-54	PerCP-eFluor 710	Invitrogen	46-5866-82	AB_2573781
Siglec-F	E50-2440	PE	BD Biosciences	552126	AB_394341
XCR1	ZET	BV421	Biolegend	148216	AB_2565230

In vivo organ uptake of TRL-mimicking particles and glucose

Mice (n=5 per group) received an intravenous injection with an emulsion of TRL-like particles (60 nm) containing glycerol tri[^{3}H]oleate (1 mg TG in 200 µL saline per mouse) prepared as described previously[3], together with 2-[1-^{14}C]-deoxyglucose (NEC495A250UC; PerkinElmer, Waltham, MA, USA) in a radioactivity ratio of ^{3}H:^{14}C = 5:1. After 15 minutes, mice were killed by CO_2 asphyxiation and perfused via the

heart with ice-cold PBS. Various organs were collected and up to approx. 300 mg per tissue dissolved in 0.5 mL Solvable (6NE9100, PerkinElmer, Waltham, MA, USA) at 56°C overnight, after which 5.0 mL Ultima Gold scintillation fluid (6013329, PerkinElmer, Waltham, MA, USA) was added. Plasma (5 µL) was directly added to 2.5 mL Ultima Gold. ^{3}H-activity and ^{14}C-activity were measured with a scintillation counter (Tri-Carb 2910 TR, PerkinElmer, Waltham, MA, USA) and expressed as a percentage of injected dose per gram tissue.

Liver and adipose tissue histology

Liver tissue and sWAT (n=16-18 per group) were fixed in 4% paraformaldehyde, dehydrated, embedded in paraffin, and sectioned (5 µm). Liver sections were stained with hematoxylin-eosin (H&E), and the MASLD score was determined according to Liang *et al* [4]. Briefly, the scoring ranges from 0 to 8 and is evaluated semi-quantitatively through three criteria: microsteatosis, macrosteatosis and hypertrophy. Each criterion is ranked from 0 to 3, where 0 = <5% of the tissue occupied, 1 = between 5% and 33% of the tissue occupied, 2 = between 33% and 66% of the tissue occupied, and 3 = >66% of the tissue occupied and the combined score of microsteatosis and macrosteatosis can maximally be 5. The inflammation score was similarly calculated from 0 to 3, where, excluding inflammatory cells around the blood vessels, the number of inflammatory foci was rated as following: 0 =<0.5 foci per visual field, 1 = between 0.5 and 1 foci, 2 = between 1 and 2 foci, and 3 = more than 2 inflammatory foci, where visual field of 3.1 mm^2 was used. For the staining of liver macrophages, endogenous peroxidase was blocked with H_2O_2, and the antigen was retrieved with proteinase K (1.24568.0500, Merck, Rahway, New Jersey USA). Treated sections were then incubated with the primary antibody (Anti-F4/80 antibody AB_1140040, ab6640, Abcam, Cambridge, UK) and a peroxidase-conjugated secondary antibody (AB_3148621, MP-7444, Vector Laboratories, Newark, USA) which was visualized using the Vector NovaRED® Substrate Kit (SK-4800). Nuclei were stained with Mayer's hemalum solution (1.09249, Sigma-Aldrich, St Louis, USA). Collagen was stained with 0.1% Direct Red 80 (365548, Sigma-Aldrich, St Louis, Missouri, USA) and 0.1% Fast Green (F7258, Sigma-Aldrich, St Louis, Missouri, USA). The MASLD score was determined by eye in 6–9 randomly selected fields (~1.5 mm^2) per sample, while F4/80-positive and collagen-positive areas were quantified in 4 randomly selected fields with ImageJ software version 1.52a (see Supplementary document 3 for the code). sWAT slides were stained with H&E, and the adipocyte size was determined with ImageJ

software, while the amount of crown-like structures was manually counted. In experiment 2, frozen cut liver sections were stained with Oil Red O staining[5] and the lipid-positive area was quantified with ImageJ software version 1.52a.

Liver lipid quantification

Hepatic lipids were extracted from snap-frozen liver samples (n=18 per group) using a modified protocol from Bligh and Dyer[6]. TG and TC were measured as aforementioned, and protein concentrations were measured using a commercial kit (Pierce BCA Protein Assay Kits, Thermo Fisher Scientific, Waltham, Massachusetts, USA). Hepatic lipid content was expressed as nmol per mg protein.

Gene expression

Total RNA was isolated from snap-frozen tissues (n=18 per group) using TriPure RNA Isolation Reagent (Roche Diagnostics, Mijdrecht, The Netherlands). cDNA was generated using Moloney Murine Leukemia Virus Reverse Transcriptase (Promega, Madison, Wisconsin, USA). Quantitative real-time PCR was performed using GoTaq® qPCR Master Mix (A6002, Promega, Madison, Wisconsin, USA) with a Bio-Rad CFX384 Touch Real-Time PCR Detection System. mRNA expression levels were normalized to ribosomal protein lateral stalk subunit P0 (*Rplp0*) using the delta-delta Ct method[7] and expressed as fold change compared with the E-SED group in experiment 1 and SED group in experiment 2. The primer sequences are listed in Table 2.

Table 2. Mouse primers used for quantitative real-time PCR.

Gene	Forward primer (5'→3')	Reverse primer (5'→3')
Cd36	GCAAAGAACAGCAGCAAAATC	CAGTGAAGGCTCAAAGATGG
Col1a1	GAGAGAGCATGACCGATGGATT	TGTAGGCTACGCTGTTCTTGCA
Cpt1a	GAGACTTCCAACGCATGACA	ATGGGTTGGGGTGATGTAGA
Cyp27a1	TCTGGCTACCTGCACTTCCT	CTGGATCTCTGGGCTCTTTG
Cyp7a1	CAGGGAGATGCTCTGTGTTCA	AGGCATACATCCCTTCCGTGA

Cyp7b1	CAGCTATGTTCTGGGCAATG	TCGGATGATGCTGGAGTATG
Cyp8b1	GGACAGCCTATCCTTGGTGA	CGGAACTTCCTGAACAGCTC
Fasn	GCGCTCCTCGCTTGTCGTCT	TAGAGCCCAGCCTTCCATCTCCTG
Il1b	GCAACTGTTCCTGAACTCAACT	ATCTTTTGGGGTCCGTCAACT
Ldlr	GCATCAGCTTGGACAAGGTGT	GGGAACAGCCACCATTGTTG
Rplp0	GGACCCGAGAAGACCTCCTT	GCACATCACTCAGAATTTCAATGG
Srebp1c	AGCCGTGGTGAGAAGCGCAC	ACACCAGGTCCTTCAGTGATTTGCT
Srebp2	TGAAGCTGGCCAATCAGAAAA	ACATCACTGTCCACCAGACTGC
Tnfa	GGCAGGTCTACTTTGGAGTCATTGC	ACATTCGAGGCTCCAGTGAATTCGG

Protein isolation and Western blot

Frozen TA muscle samples (approx. 30-40 mg) from mice of experiment 1 were lysed in a freshly prepared PI3K buffer with protease and phosphatase inhibitors (A32959, Thermo Fisher Scientific, Waltham, MA, USA), and homogenized using a ZentriMix 380 R (Andreas Hettich GmbH & Co. KG, Tuttlingen, Germany) twice at 2000 rcf for 1 min. Samples were centrifuged three times (16200 rcf for 5 min at 4°C) to ensure the fat removal. Protein concentrations in the supernatant were determined using the Pierce™ BCA Protein Assay Kit (23225, Thermo Fisher Scientific, Waltham, MA, USA), according to the manufacturer's protocol. 10 µg of protein per sample was loaded on NuPAGE™ 4-12%, Bis-Tris, 1.0–1.5 mm, Mini Protein Gels (NP0329PK2 Thermo Fisher Scientific, Waltham, MA, USA) and proteins were separated in a Mini Gel Tank (A25977, Thermo Fisher Scientific, Waltham, MA, USA). Proteins were then blotted on a PVDF membrane with a Trans-Blot Turbo Transfer System (Bio-Rad Laboratories, Hercules, CA, USA). The membrane was stained with Ponceau S (A40000279, Thermo Fisher Scientific, Waltham, MA, USA) for total protein abundance quantification, blocked in 5% milk in TBS-T, washed in TBS-T, and incubated first overnight with a Total OXPHOS Rodent WB Antibody Cocktail (AB_2629281, ab110413, Abcam, Cambridge, UK) and then with an anti-mouse HRP-conjugate secondary antibody for 1 hour at room temperature (AB_430834, W4021. Promega, Madison, Wisconsin, USA). The bands were visualized using a

SuperSignal™ West Pico PLUS Chemiluminescent Substrate (34580, Thermo Fisher Scientific, Waltham, MA, USA) and measured with a ChemiDoc™ Touch Imaging System (Bio-Rad Laboratories, Hercules, CA, USA). The bands were normalized to total protein loading.

Plasma short-chain fatty acid quantification

Eight SCFAs were quantified in portal vein plasma (n=6 per group) collected in experiment 1: acetic acid (C2), propionic acid (C3), isobutyric acid (C4), butyric acid (C4), 2-methyl-butyric acid (C5), isovaleric acid (C5), valeric acid (C5) and caproic acid (hexanoic acid, C6) by LC-MS/MS by Metabolon Inc. (North Carolina, USA; Metabolon Method TAM148: "LC-MS/MS Method for the Quantitation of Short Chain Fatty Acid (C2 to C6) in Human Plasma and Serum"). Plasma samples were spiked with stably labelled internal standards and were homogenized and subjected to protein precipitation with an organic solvent. After centrifugation, an aliquot of the supernatant was derivatized. An aliquot of the reaction mixture was injected onto an Agilent 1290/AB Sciex QTrap 5500 LC MS/MS system equipped with a C18 reversed phase UHPLC column. The mass spectrometer was operated in negative mode using electrospray ionization (ESI). The peak area of the individual analyte product ions was measured against the peak area of the product ions of the corresponding internal standards. Quantitation was performed using a weighted linear least squares regression analysis generated from fortified calibration standards prepared concurrently with study samples. LC-MS/MS raw data was collected and processed using AB SCIEX software Analyst 1.7.3 and processed using SCIEX OS-MQ software v3.0.

Bomb calorimetry

For feces collection, mice (experiment 1) were put into clean empty cages for 20 minutes every 6 hours for 24 hours. Feces were collected per cage, placed immediately on dry ice and then freeze-dried for 48 hours. Around 150 mg of freeze-dried feces (pooled equally from each time point) were pulverized and used to determine caloric content by an oxygen bomb calorimeter (6100 Compensated Calorimeter, Parr Instrument Company, Moline, Illinois, USA).

16S sequencing and metagenomic sequencing

All cecum content samples from experiment 1, and nine representative samples per group from experiment 2 (mice that had the closest MASLD score and liver TG

concentration to the average of the group) were used for 16S sequencing. 30 ng qualified DNA isolated from mouse cecum content and 16S v3-v4 pair-end Amplicon Sequencing primers (338F forward primer: ACTCCTACGGGAGGCAGCAG; 806R reverse primer: GGACTACHVGGGTWTCTAAT) were added for PCR. All PCR products were purified by Agencourt AMPure XP beads (Beckman Coulter, Inc, Brea, California, USA), dissolved in Elution Buffer and eventually labeled to finish library construction. Library size and concentration were detected by Agilent 2100 Bioanalyzer. Qualified libraries were sequenced on the DNBSEQ-G400 platform according to their insert size. The QIIME 2 2021.8 tool was used to process the data and statistical analyses were performed in R version 4.1.1. Briefly, the raw sequence data were denoised and quality filtered with the DADA2 plugin (via "denoise-paired")[8]. The obtained representative sequences were classified with the feature-classifier plugin (via "classify-sklearn")[9] using the pre-trained Silva 138.1 animal-distal-gut taxonomy classifier. For the statistical analyses, the Phyloseq package (version 1.36.0)[10] was used to integrate the counts matrix, taxonomy and metadata. To determine α-diversity (presented as Shannon index), the package's function "estimate richness" was used and a one-way ANOVA was performed to compare the groups. Bray–Curtis dissimilarity index was used to calculate the β-diversity, with PERMANOVA testing to quantify the differences between the groups. For the identification of taxa changed between the groups, DESeq2[11] (version 1.44.0) and SIAMCAT[12] (version 1.12, abundance filtering = 0.01) were used with a false discovery rate correction = 0.05. Results are shown if the adjusted p-value was below 0.05. Ggplot2 (version 3.3.5)[13] was used for all visualizations of the 16S sequencing data. On a subset of cecum content DNA samples (n = 5-6 per group, samples that had the closest MASLD scores to the group average), metagenomic shotgun sequencing was performed on the DNBSEQ platform with a paired-end sequencing read length of 150bp. Raw data with adapter sequences or low-quality sequences was filtered. Valid data was obtained after data processing using the SOAPnuke software developed by BGI. These data were then processed using NGLess version 1.0[14] with the mOTU-tool (version 2.6) module[15] and statistical analyses were performed in R version 4.1.1 similarly to 16S analysis. In all analysis, default functions' parameters were used unless stated otherwise.

Supplementary references:

1. Schonke M, Ying Z, Kovynev A, et al. Time to run: Late rather than early exercise training in mice remodels the gut microbiome and reduces atherosclerosis development. *FASEB J*. Jan 2023;37(1):e22719. doi:10.1096/fj.202201304R
2. van der Zande HJP, Gonzalez MA, de Ruiter K, et al. The helminth glycoprotein omega-1 improves metabolic homeostasis in obese mice through type 2 immunity-independent inhibition of food intake. *Faseb Journal*. Feb 2021;35(2)doi:10.1096/fj.202001973R
3. Ying ZX, Boon MR, Coskun T, Kooijman S, Rensen PCN. A simplified procedure to trace triglyceride-rich lipoprotein metabolism. *Physiol Rep*. Apr 2021;9(8)doi:10.14814/phy2.14820
4. Liang W, Menke AL, Driessen A, et al. Establishment of a general NAFLD scoring system for rodent models and comparison to human liver pathology. *PLoS One*. 2014;9(12):e115922. doi:10.1371/journal.pone.0115922
5. Du JB, Zhao L, Kang Q, He Y, Bi Y. An optimized method for Oil Red O staining with the salicylic acid ethanol solution. *Adipocyte*. Dec 31 2023;12(1)doi:10.1080/21623945.2023.2179334
6. Liu C, Schönke M, Spoorenberg B, et al. FGF21 protects against hepatic lipotoxicity and macrophage activation to attenuate fibrogenesis in nonalcoholic steatohepatitis. *Elife*. Jan 17 2023;12doi:10.7554/eLife.83075
7. Livak KJ, Schmittgen TD. Analysis of relative gene expression data using real-time quantitative PCR and the 2(-Delta Delta C(T)) Method. *Methods*. Dec 2001;25(4):402-8. doi:10.1006/meth.2001.1262
8. Callahan BJ, McMurdie PJ, Rosen MJ, Han AW, Johnson AJA, Holmes SP. DADA2: High-resolution sample inference from Illumina amplicon data. *Nat Methods*. Jul 2016;13(7):581-+. doi:10.1038/Nmeth.3869
9. Bokulich NA, Kaehler BD, Rideout JR, et al. Optimizing taxonomic classification of marker-gene amplicon sequences with QIIME 2's q2-feature-classifier plugin. *Microbiome*. May 17 2018;6doi:10.1186/s40168-018-0470-z
10. McMurdie PJ, Holmes S. phyloseq: An R Package for Reproducible Interactive Analysis and Graphics of Microbiome Census Data. *Plos One*. Apr 22 2013;8(4)doi:10.1371/journal.pone.0061217

11. Love MI, Huber W, Anders S. Moderated estimation of fold change and dispersion for RNA-seq data with DESeq2. *Genome Biol*. 2014;15(12)doi:10.1186/s13059-014-0550-8
12. Wirbel J, Zych K, Essex M, et al. Microbiome meta-analysis and cross-disease comparison enabled by the SIAMCAT machine learning toolbox. *Genome Biol*. Mar 30 2021;22(1)doi:10.1186/s13059-021-02306-1
13. Villanueva RAM, Chen ZJ. ggplot2: Elegant Graphics for Data Analysis, 2nd edition. *Meas-Interdiscip Res*. 2019;17(3):160-167. doi:10.1080/15366367.2019.1565254
14. Coelho LP, Alves R, Monteiro P, Huerta-Cepas J, Freitas AT, Bork P. NG-meta-profiler: fast processing of metagenomes using NGLess, a domain-specific language. *Microbiome*. Jun 3 2019;7doi:10.1186/s40168-019-0684-8
15. Milanese A, Mende DR, Paoli L, et al. Microbial abundance, activity and population genomic profiling with mOTUs2. *Nat Commun*. Mar 4 2019;10doi:10.1038/s41467-019-08844-4